Desynchronization between timers provokes transient arrest during *C. elegans* development

Short title: Active timer resynchronization during development

Francisco J. Romero-Expósito[1], Almudena Moreno-Rivero[1], Marta Muñoz-Barrera[1], Sabas García-Sánchez[1], Fernando Rodríguez-Peris[1], Nicola Gritti[2], Francesca Sartor[3], Martha Merrow[3], Jeroen S. van Zon[2], Alejandro Mata-Cabana[1] and María Olmedo[1,*]

[1] Departamento de Genética, Facultad de Biología, Universidad de Sevilla, Spain.
[2] AMOLF, Amsterdam, The Netherlands.
[3] Institute of Medical Psychology, Faculty of Medicine, LMU Munich, Germany.

[4] Correspondence: mariaolmedo@us.es
Keywords: Insulin, RAS, Proliferation, Arrest, Developmental timers

Field codes: Development

ABSTRACT

In multicellular organisms, developmental timers integrate internal and external cues to control numerous cellular processes that need to be temporally coordinated. The molting timer and the developmental timer run in parallel during *C. elegans* development. We reveal a novel state of transient arrest of the molting timer upon delay of the developmental timer. This means that synchronous development is not inherent but requires active synchronization of parallel timers. Additional timer variability, like that provoked by modulation of nutrient sensing pathways, increases desynchrony between these timers and consequently extends transient arrest. Mutation of the insulin receptor gene *daf-2* reduces the speed of both timers but has a larger impact on the developmental timer, that then appears delayed relative to the molting timer. In this context, prolonged arrest of the molting timer provides a mechanism for resynchronization.

Teaser

Active resynchronization at specific checkpoints of two parallel timers controlling developmental events.

INTRODUCTION

Development is a temporal program made up of different modules that typically proceed in a precise series of events. To achieve reproducible development, organisms must integrate information from intrinsic developmental timers with external cues, such as changes in nutrition and temperature. During the postembryonic development of *C. elegans*, each larval stage is defined by distinct cellular events of division, migration, and differentiation. These events have been meticulously traced due to the highly consistent nature of the process. Seam cells divide asymmetrically, approximately at the beginning of each larval stage. In the second larval stage (L2) there is, in addition, a symmetric division before the asymmetric division (*1*). Additionally, a reiterative process of molting takes place over each of the four larval stages (L1-4), each of them consisting of an intermolt (I1-4) and a molt (M1-4). Molting is a period defined by a sleep-like stage of behavioral quiescence (*2*) and by the generation of a new cuticle. At the end of the molt, larvae shed their old cuticle in a process known as ecdysis (*3*). Cell divisions and molting show an apparent coordination, with events taking place in an orderly manner. However, the events of cell division and molting seem to be controlled by independent timers that can be uncoupled (*4*), leading to alterations in the characteristic sequence (*5*). These timers, regulating cell divisions and molting, are respectively referred to as the developmental timer and the molting timer (*4*).

Multiple factors related to nutrition regulate the duration of each stage of development (*5*-*8*). One of the major pathways controlling of *C. elegans* development is that for Insulin/IGF-1 signaling (IIS). This nutrient sensing pathway controls lifespan and developmental progression and is conserved across metazoans. In *C. elegans*, the gene *daf-2* encodes the sole insulin receptor DAF-2/IR. Canonical signaling through the pathway involves the phosphatidylinositol-3-OH kinase (PI3K) AGE-1, and the serine/threonine kinases PDK-1, AKT-1, and AKT-2. These proteins regulate the activity of the transcription factor (TF) DAF-16/FOXO. Reduced DAF-2 function leads to increased lifespan in a DAF-16 dependent manner, suggesting that this TF is the main effector of the pathway (reviewed in (*9*)). Hypomorphic *daf-2* alleles also show stage-specific developmental delays (*6*, *8*). While all larval stages are prolonged in the *daf-2(e1370)* mutant, the L1 stage shows reduced sensitivity to insulin signaling levels. The delays of the *daf-2* mutant have been quantified at the level of molting, but the insensitivity of L1 seems to be due to the specific cell fates of this larval stage (*6*). These observations suggest that DAF-2 controls the speed of both the developmental and the molting timer.

Robust development requires coordination between cell divisions and their differentiation, and organismal growth (reviewed in (*10*)). Since the two *C. elegans* timers are independent, reduced insulin signaling could impact the timers identically to maintain coordination between them while reducing the speed of the process. Alternatively, both timers may also run at different speeds upon lowered insulin signaling requiring a mechanism to restore synchronization. We aim to characterize novel developmental features that will distinguish mechanisms of synchronization.

To this end, we have used a method for time-resolved analysis of the developmental process. By monitoring the molting timer at high temporal resolution (5-minute time points), we show a state of transient arrest at the beginning of the larval stages. Hypomorphic *daf-2* mutants have longer transient larval arrests of the molting timer compared to the wild type. Focusing on the arrest at the beginning of the second larval stage (L2a), we show that this phenotype is partially independent of DAF-16/FOXO. Mutation of *daf-18*, encoding the tumor suppressor DAF-18/PTEN,

reduces transient larval arrest. While the *daf-18* mutation completely rescues other developmental phenotypes of *daf-2*, features of transient larval arrest indicate that it is not entirely dependent on DAF-18. Additionally, we have uncovered a role for RAS signaling in L2a transient arrest. Reduction of *mpk-1* by RNAi increases transient arrest at the beginning of the second larval stage. Conversely, a *let-60* gain of function mutation reduces it in all backgrounds tested. RAS mutants also impacted the duration of the first larval stage. Larvae treated with *mpk-1* RNAi progress faster through L1 but to arrest for longer times. Similarly, *let-60(gf)* mutants progress more slowly than the wild type through L1 and show a shorter transient arrest. This led us to hypothesize that L2a could be the consequence of desynchrony between the molting and the developmental timers at the end of the first larval stage. Indeed, the mutation *daf-2(e1370)* impacts both the developmental and the molting timers, but the delay in cell divisions is greater than that of the larval stages, resulting in desynchrony between timers at the transition between L1 and L2. The mutation *daf-18* reduces desynchrony between the timers of *daf-2* mutants by accelerating the developmental timer.

By combining two reporter systems to monitor transient arrest and cell division in the same animal, we observed that larvae in L2a present a delay in seam cell division relative to ecdysis. This observation links transient arrest and timer desynchrony. Importantly, experimental delay of the molting timer results in reduced transient arrest, while delay of the developmental timer increases it, suggesting that the delay of the developmental timer relative to ecdysis provokes the transient arrest of the molting timer. Our results support a model in which the transient arrest of the molting timer allows a delayed developmental timer to catch up so that desynchrony generated by a slow timer does not amplify over the process of postembryonic development.

RESULTS

A transient arrest of the molting timer

Analysis of postembryonic development in *C. elegans* has often relied on observation of morphological changes. Here, we applied a high-throughput, quantitative method to measure development (*11*) that allows unveiling unknown complexities on the timing of the different larval stages (*6*, *12*, *13*). This method relies on the use of the enzyme Luciferase, which is constitutively expressed in a *C. elegans* reporter strain (*11*). Luciferase catalyzes the oxidation of Luciferin, in a reaction that emits light (*14*). We provide Luciferin in the media of the developing larvae, so that food intake results in emission of light. When larvae stop feeding during the molting periods, the emission of light decreases rapidly, generating a characteristic profile that is used to calculate the duration of each larval stage, allowing identification of intermolts (I) and molts (M) (Fig. 1A) (*11*).

In the analysis of developmental phenotypes of the *daf-2(e1370)* allele, we observed a novel feature of postembryonic development. In addition to the overall developmental delay previously described for this mutant, we detected a decrease in the bioluminescence signal immediately after ecdysis (Fig. 1B, middle and right). To quantify this feature of development, we defined the periods L2a, L3a, and L4a, which respectively appeared at the beginning of the L2, L3, and L4. Each of these periods comprises the time from the end of the previous molt to the point when bioluminescence recovers to the levels that are typical of larval stages (Fig. 1C). This novel feature of development also appears in the wild-type strain, although at a lower frequency (approximately in 60% of the larvae vs. 90%) and with shorter duration than in *daf-2* (Fig. 1D-E). Here, we focus our analysis on L2a, as this is the stage with the longest average duration, especially for the wild-type strain. A key feature of L2a is that, unlike molts and intermolts, the

duration of these periods shows high inter-individual variability. We compared the L2a with the previous and subsequent stages, M1 and *bonafide* l2 respectively, with *bonafide* l2 being the duration of the second intermolt after subtracting the L2a period (Fig. 1C). For individual worms, the duration of the stage relative to the population average is close to 1 for M1 and *bonafide* l2, but it ranges from 0 to 4 for the L2a stage (Fig. 1F). The coefficient of variation increases around tenfold in L2a compared to the previous and following stages (Fig. 1 G). Furthermore, when we observe abnormally long intermolts, subtracting the duration of the L2a results in similar durations of the *bonafide* intermolt (Fig. 1 H). Therefore, the periods in L2a seem to be added to the average duration of larval stages, suggesting that they correspond to a state of developmental arrest. However, another feature suggests that L2a is not a complete developmental arrest. Both entry and exit from this state occur spontaneously, without any change in environmental conditions, indicating that during L2a development is still ongoing at some level. These results suggest that L2a corresponds to a transient arrest of the molting timer provoked by the internal state of the larva. Transient arrest occurs even in the wild-type strain in food replete conditions.

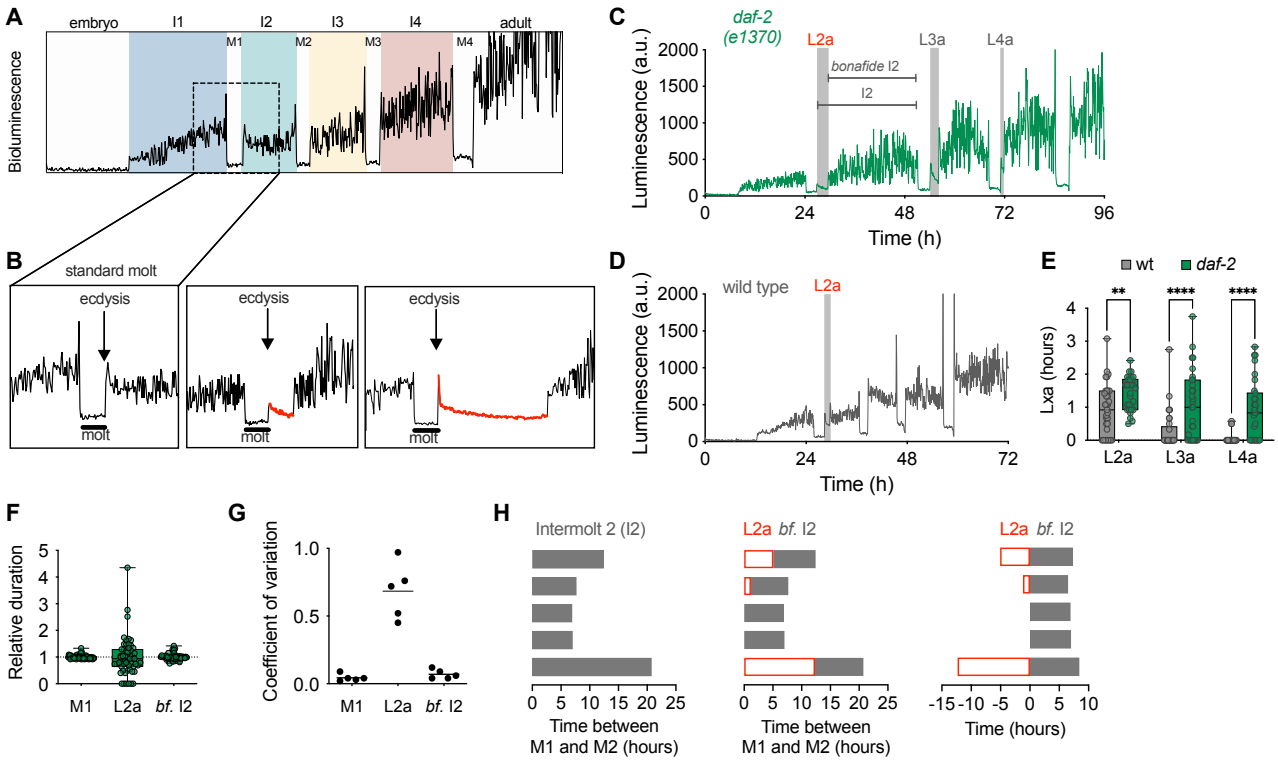

Figure 1. *daf-2(e1370)* shows a novel developmental phenotype. (A) Representative profile of luminescence over late embryonic and the complete postembryonic development **(B)** Zoom in of a standard molt (left) and profiles showing representative short and long periods of transient arrest (center and right). **(C, D)** Representative profile of luminescence of the *daf-2(e1370)* (B) and wild-type strain (C), indicating the presence of the L2a stage. **(E)** Duration of the transient larval arrest in the wild type and *daf-2(e1370)* larvae. Statistical differences show Fisher´s LSD between strains after two-way ANOVA, ** p<0.01, **** p<0.0001. The dots show individual larvae in 3 independent experiments. Complete report of replicates and statistics results is shown in Table S2 and File S1. **(F)** Duration of M1, L2a and *bonafide* l2 relative to the average duration of each stage for 56 *daf-2* mutant larvae in 5 independent experiments. **(G)** Coefficient of variation per experiment (CV) for each of the intervals shown in E. **(H)** Duration of the second intermolt (l2) for selected animals with average and extreme values (left) and representation of the corresponding periods of L2a and *bonafide* l2 (center and right).

Transient larval arrest increases in *daf-2* Class 2 alleles

To understand the regulation of transient arrest, we decided to investigate whether this phenotype appeared in other *daf-2* alleles. The *daf-2* alleles have been classified in two groups attending to their phenotypes. Class 1 alleles constitutively form dauer (Daf-c), are long lived (Age) and show increased intrinsic thermotolerance (Itt). Class 2 alleles present these phenotypes and one or several other phenotypes including early larval arrest, reduced feeding (Eat) and production of progeny late in life (*15*). This classification does not reflect severity of the alleles, rather, seems to suggest that DAF-2 has several functional domains that interact with different signaling outputs (*15*, *16*).

We first tested several Class 1 *daf-2* alleles at 20 ºC, as we did earlier for the Class 2 allele *e1370*. From the alleles tested in this experiment, we could not find significant differences in L2a relative to the wild-type strain. However, in this condition, most of these alleles show mild developmental phenotypes compared to *daf-2(e1370)* (Fig. S1A,B). To reveal the phenotypes of Class 1 *daf-2* alleles we raised the cultivation temperature to 22.5 ºC. At this temperature, all the *daf-2* alleles tested showed a significant increase in the duration of the second intermolt (I2) (Fig. 2A), but not in the average duration of the L2a stage (Fig. 2B). In addition to the lack of statistically significant impact on L2a duration, the change in L2a duration for the different mutants did not correlate with the duration of the I2. For example, the allele *m596* showed a three-fold increase in the duration of I2 compared to the wild-type, while showing a similar value of L2a (Fig. 2A,B). These observations suggest that these two phenotypes of *daf-2(e1370)* - increased I2 and increased L2a - are independent from each other. On the other hand, when we tested the class 2 alleles *e979* and *e1391,* we observed increased values of L2a along with the I2 extension (Fig. 2C,D). Overall, our analysis shows that increased transient larval arrest is a phenotype of Class 2 *daf-2* alleles.

We also analyzed developmental phenotypes resulting from degradation of DAF-2 using a strain with a tag for auxin induced degradation (AID) at the endogenous *daf-2* locus (*17*). At concentrations of 2 and 4 μM of the auxin analog NAA (1-Naphthaleneacetic acid), the duration of the second intermolt was similar to that of the *daf-2(e1370)* mutant (Fig. 2E). Importantly, those concentrations only impacted the duration of I2 in a strain expressing TIR1, which is necessary for NAA-mediated degradation of the target protein DAF-2 (Fig. S1C). In this strain, the duration of I2 increases with the amount of NAA, showing that the extent of DAF-2 degradation affects the duration of the stage (Fig. 2E). However, the duration of the L2a after DAF-2 degradation was similar to that of the wild-type (Fig. 2F). The efficiency of the DAF-2 degradation before the L2a is demonstrated by the developmental delay observed in I1, which is stronger than that of the *daf-2* mutant (Fig. S1D). This result shows that degradation of DAF-2 does not have the same effect on L2a as the impairment of function caused by the *daf-2(e1370)* mutation. In conclusion, specifically *daf-2* Class 2 alleles alter insulin signaling to increase transient larval arrests.

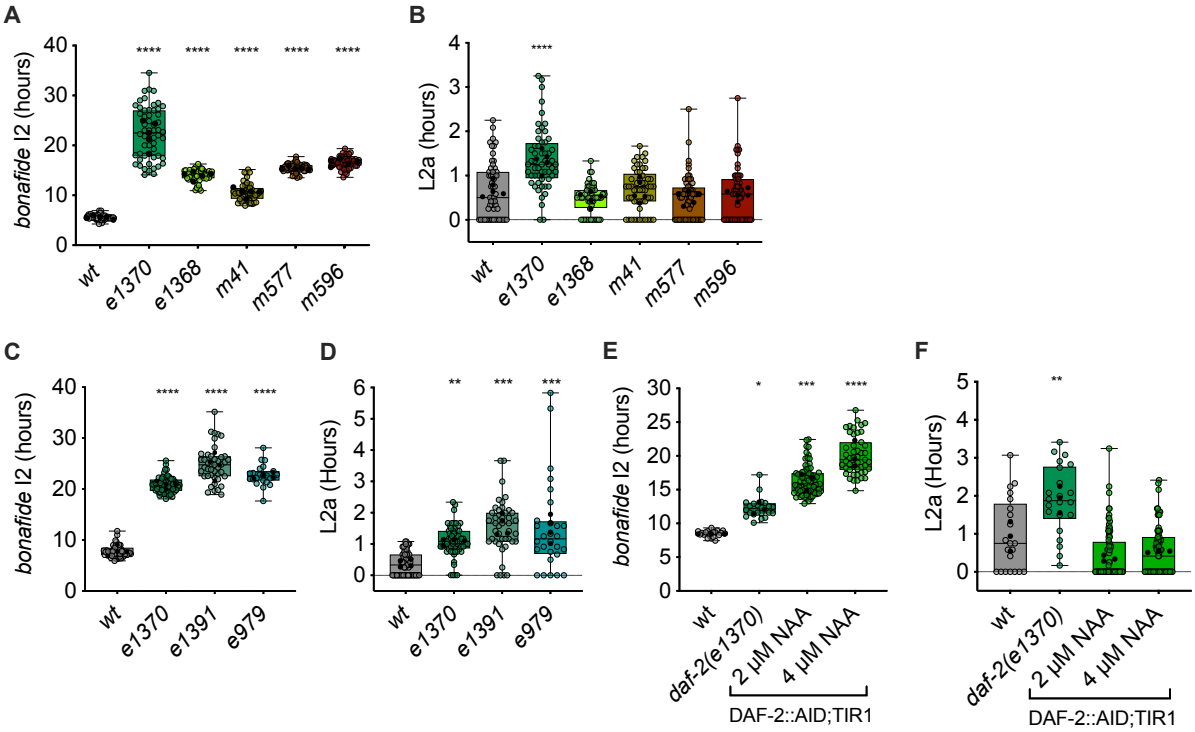

Figure 2. Transient larval arrest increases in *daf-2* Class 2 alleles. (A, B) Duration of the *bonafide* l2 (A), and L2a (B) at 22.5 ºC, in the wild-type strain, *daf-2(e1370)*, and the *daf-2* class 1 alleles *e1368*, *m41*, *m577,* and *m596,* from five independent experiments. **(C, D)** Duration of the *bonafide* l2 (C), and L2a (D), in the wild-type strain and the *daf-2* class 2 alleles *e1370*, *e1391* and *e979,* from four independent experiments. **(E, F)** Duration of the *bonafide* l2 (E), and L2a (F) of the wild-type strain, *daf-2(e1370)*, and a strain containing an AID tagged version of DAF-2 and expressing TIR1 under the somatic promoter P*eft-3* (DAF-2::AID,TIR1) on the presence of 2 and 4 µM NAA, in three independent experiments. Colored circles show values for individual larvae and black dots show the average for each experiment. For all panels, we compared the averages of each mutant to that of the wild type using One-way ANOVA followed by Dunnet´s multiple comparisons. Complete report of replicates and statistics results is shown in Table S2 and File S1. Only significant differences are shown and are marked as * p<0.05, ** p<0.01, ***p<0.001, **** p<0.0001.

The L2a phenotype of *daf-2(e1370)* is partially independent from the rest of IIS

The Class 2 specificity of the L2a phenotype suggests that the DAF-2 receptor might communicate with more than one pathway. Most *daf-2* phenotypes are mediated by the activation of DAF-16 (Fig. 3A), and they are rescued in a double *daf-2;daf-16* mutant. Thus, phenotypes observed in *daf-2* mutants as constitutive dauer formation, lifespan extension, and the increased duration of the L2 stage, are absent in the double mutant *daf-2(e1370)*;*daf-16(mu86)* (*8*, *18*, *19*). Indeed, we observed that both *daf-16* and the double *daf-2;daf-16* mutants show a duration of the second intermolt similar to the wild-type strain (Fig. 3B). Therefore, the extension of this stage in the *daf-2(e1370)* mutant requires the function of DAF-16. However, when we quantified L2a, we observed that *daf-16* has similar levels to the wild-type strain but the double mutant *daf-2;daf-16* shows L2a levels intermediate between the wild type and the *daf-2* mutant (Fig. 3C). We then analyzed the double mutants *daf-2;daf-16* for the other two Class 2 alleles, *e1391* and *e979*. For both alleles, *daf-16* suppressed completely the longer l2 completely, but only partially suppressed partially the L2a phenotype (Fig. S2 A-D). These results show that part of the impact of the *daf-2* mutation is independent of DAF-16. Also, it reinforces the idea that the transient larval arrest phenotype is independent of other developmental phenotypes of *daf-2*.

To understand at what level of IIS the signal from DAF-2 bifurcates to other pathways, we focused on AGE-1/PI3K, which receives the signal from the receptor. AGE-1 phosphorylates PIP_2 to form PIP_3 (phosphatidylinositol 3,4,5-triphosphate[PI(3,4,5)P3]) (*20*). PIP_3 is required for activation of downstream components of IIS (Fig. 3A). We measured development of the mutant *age-1(mg305)* and observed a longer duration of both developmental stages and transient larval arrest (Fig. 3D-E). This mutant, as *daf-2(e1370),* is a hypomorphic allele, making it difficult to compare the effect of the two mutations, as the extent of the phenotype might be due to the severity of the specific allele. However, while the phenotype of *age-1* is more severe for the duration of the intermolt I2 than that of the *daf-2(e1370)* mutant, the L2a phenotype is milder. Furthermore, unlike for *daf-2*, the *daf-16* mutation completely suppressed the effect of the *age-1* mutation, as the double mutant *age-1;daf-16* is undistinguishable from the wild type and the *daf-16* mutant (Fig. 3D-E). These results imply that the *age-1* phenotype is completely DAF-16 dependent, suggesting that part of the signal from the DAF-2 receptor to bypass larval transient arrest bifurcates to other pathways prior to AGE-1.

DAF-18/PTEN promotes transient larval arrest

The wild-type strain shows a basal level of L2a. It could be that the wild-type level of IIS signaling leads to some level of DAF-16 activation, but the *daf-16* mutation does not reduce the wild-type levels of L2a (Fig. 2C, E, G). Looking for additional regulators of the process, we focused on DAF-18, which counteracts insulin signaling by dephosphorylating the PIP_3, opposing the effect of AGE-1 (*21*) (Fig. 3A), but also acts independently of AGE-1 and DAF-16. Besides its lipid phosphatase function, DAF-18/PTEN also presents protein phosphatase activity. PTEN can dephosphorylate the Insulin Receptor (IR) and the IR inhibits PTEN (*22*).

We tested the effect of the deletion allele *daf-18(ok480)* in the developmental phenotypes observed previously. The *daf-18* mutation does not provoke any changes in the duration of the second intermolt in a background wild-type for *daf-2* [*daf-2 (+)*], similarly to *daf-16* (Fig. 3F). However, both mutations suppressed the developmental delay of the *daf-2* mutant [*daf-2 (-)*] (Fig. 3F). This result implies that DAF-18 and DAF-16 act in a linear pathway antagonizing the role of DAF-2 in the duration of the larval stages. For the regulation of larval transient arrest, the situation is different. First, the *daf-18* mutant reduces the duration of the L2a measured in the wild-type background [*daf-2 (+)*] (Fig. 3G), reinforcing the idea that the duration of larval stages and that of the transient larval arrest are regulated by different mechanisms. The *daf-2* mutation increases the duration of L2a in all backgrounds. Importantly, the difference between the *daf-2* mutant and the double *daf-2;daf-16* (marked as c) disappears when combined with the *daf-18* mutation (*daf-2;daf-18* vs. *daf-2;daf-16;daf-18*, marked as d) (Fig. 3G). Since DAF-16 acts downstream of DAF-18 in canonical IIS, these results suggest that, for L2a, the DAF-16-independent fraction of the *daf-2* phenotype requires a function of DAF-18 and that this function is independent of its role in the canonical IIS. Despite the reduction on L2a, both the double *daf-2;daf-18* and the triple mutant *daf-2;daf-16;daf-18* show longer L2a than *daf-18 and daf-16;daf-18* (Fig. 3G), which suggests that DAF-2 signals through yet another pathway independently of DAF-18 and DAF-16.

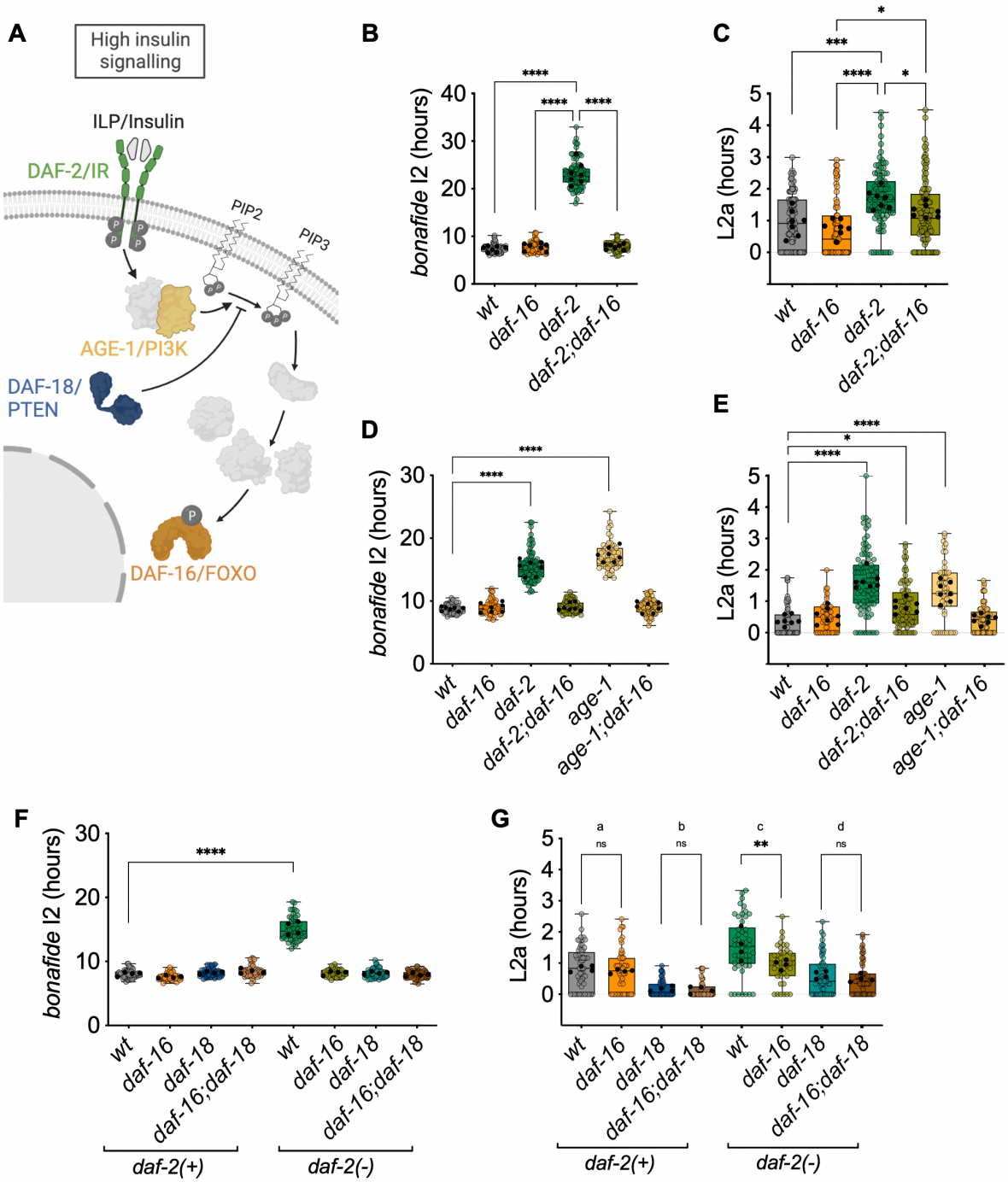

Figure 3. Reduced IIS leads to L2a by DAF-16 and DAF-18 dependent and independent pathways. (A) Representation of canonical IIS in conditions of high insulin signaling. Under low insulin signaling, as in a *daf-2* mutant, signaling through the pathway is reduced, maintaining DAF-16 in a non-phosphorylated state that results in translocation to the nucleus. **(B, C)** Duration of the *bonafide* l2 (B), and L2a (C), in the wild-type strain, *daf-16(mu86)*, *daf-2(e1370)*, and the double mutant *daf-2;daf-16*, from 8 independent experiments. **(D, E)** Duration of the *bonafide* l2 (D), and L2a (E), for the same strains as shown in B and C, and the mutants *age-1(mg305)* and *age-1;daf-16*, from seven independent experiments. **(F, G)** Duration of the *bonafide* l2 (F), and L2a (G), for the wild type, *daf-2*, *daf-16*, *daf-18*, and the respective double and triple mutants. Colored circles show values for individual larvae and black dots show the average for each experiment. For all panels, we performed One-way ANOVA followed by Tukey´s multiple comparisons to test differences between all strains. For B and C all significant differences are shown. For D-F only significant differences to the wild type are shown and marked as * p<0.05, ** p<0.01, ***p<0.001, **** p<0.0001. For G, only the results from comparing the effect of the *daf-16* mutation are shown (a-d), marked as ns >0.5, and ** p<0.01, ***p<0.001, **** p<0.0001. Complete report of replicates and statistics results is shown in Table S2 and File S1.

We also analyzed a nonsense allele of *daf-18*. The mutation *daf-18(e1375)* fully suppresses the constitutive dauer formation of class 1 *daf-2* alleles independently of their severity but showed reduced suppression of *daf-2* class 2 alleles (*16*). When we measured development of this mutant alone, and in combination with *daf-2(e1370)*, we observed that *daf-18(e1375)* completely suppresses the defect of *daf-2* in terms of the duration of the second intermolt (I2), as did the *daf-18(ok480)* (Fig. S2E). However, the impact of *daf-18(e1375)* on L2a was different to that of *daf-18(ok480)*. *daf-18(e1375)* did not reduce the L2a observed in the wild-type strain (Fig. S2F), which according to our previous results is independent of DAF-16. Furthermore, in combination with *daf-2(e1370)*, the *daf-18(e1375)* mutation provoked only a partial reduction of L2a compared to *daf-18(ok480),* similar to the phenotype of *daf-2;daf-16* mutants (Fig. S2F). These results suggest that *daf-18(e1375)* impacts I2 and L2a only through canonical IIS. In summary, DAF-18 contributes to reducing transient larval arrest through canonical-IIS-dependent and -independent pathways.

Increased RAS signaling contributes to suppression of L2a

In order to identify additional pathways that provoked the *daf-2* L2a phenotype independently of canonical IIS, we turned to RAS signaling for several reasons. First, in the *C. elegans* germline, the DAF-2 receptor activates MPK-1(ERK) during Meiotic Prophase I (*23*). Second, DAF-2 induces, and DAF-18 represses RAS signaling in the vulval precursor cells, and this role of DAF-18 is independent of other components of canonical IIS (*24*). Third, DAF-18 negatively regulated MPK-1 to inhibit germline stem cell (GCS) proliferation (*25*). This information suggested that the roles of DAF-2 and DAF-18 that are independent of canonical IIS could converge on RAS signaling.

We first analyzed the impact of reduced *mpk-1*. Treatment with *mpk-1* RNAi did not change the duration of the second intermolt (*bf.* I2) (Fig. 4A), but it increased the duration of the transient larval arrest (Fig. 4B). This result confirms that these two features of development are independent. We then reasoned that, if RAS contributes to transient larval arrest upstream of MPK-1, a gain of function allele of LET-60/RAS should reduce L2a. We used the thermosensitive gain-of-function allele *ga89,* and measured development at 22.5 ºC. *let-60(gf)* does not reduce the duration of the second intermolt in the wild-type background, nor in the *daf-2* mutant (Fig. 4C). However, *let-60(gf)* reduces the duration of L2a in the wild-type and the *daf-2* mutant backgrounds, and shows the same trend in *daf-18* and *daf-2;daf-18* (Fig. 4D). Interestingly, we also observed that the duration of L1 was increased by the gain of function mutation in *let-60(gf)* (Fig. 4E). This is a remarkable observation, as we have previously observed that the L1 stage is generally less sensitive the interventions that limit developmental rate (*6*). Indeed, in the context of insulin signaling and all the mutants analyzed previously, we never found a similar impact on L1. For instance, the reduction of L2a of all backgrounds by the *daf-18* mutation (Fig. 3D, S3A) does not correlate with an increased duration of L1 (Fig. S3B). Additionally, *mpk-1* RNAi, which increases L2a also impacts L1, in this case reducing its duration (Fig. 4F). These results suggest that the modulation of the L2a phenotype by IIS (including DAF-2, DAF-16 and DAF-18) and RAS (including LET-60 and MPK-1) might involve different mechanisms.

Since L2a transient arrest occurs immediately after the end of the first larval stage, the results from RAS regulation suggests that, when the molting timers runs faster through L1, as in *mpk-1* RNAi, this timer arrests for a longer time at the end of this stage. However, when the molting timer runs slower through L1, as in *let-60(gf),* the timer is arrested for a shorter time. Even more,

for the same *let-60(gf)* mutation, transient arrest did not increase for the L3a and L4a, as the previous stages intermolts did not shorten relative to the wild type (Fig. S3C-E). One reason for the molting timer to arrest after a fast L1 is that other processes that take place during the first stage did not have time to complete. We therefore hypothesized that transient arrest could arise from desynchronization between the molting timer and the developmental timer.

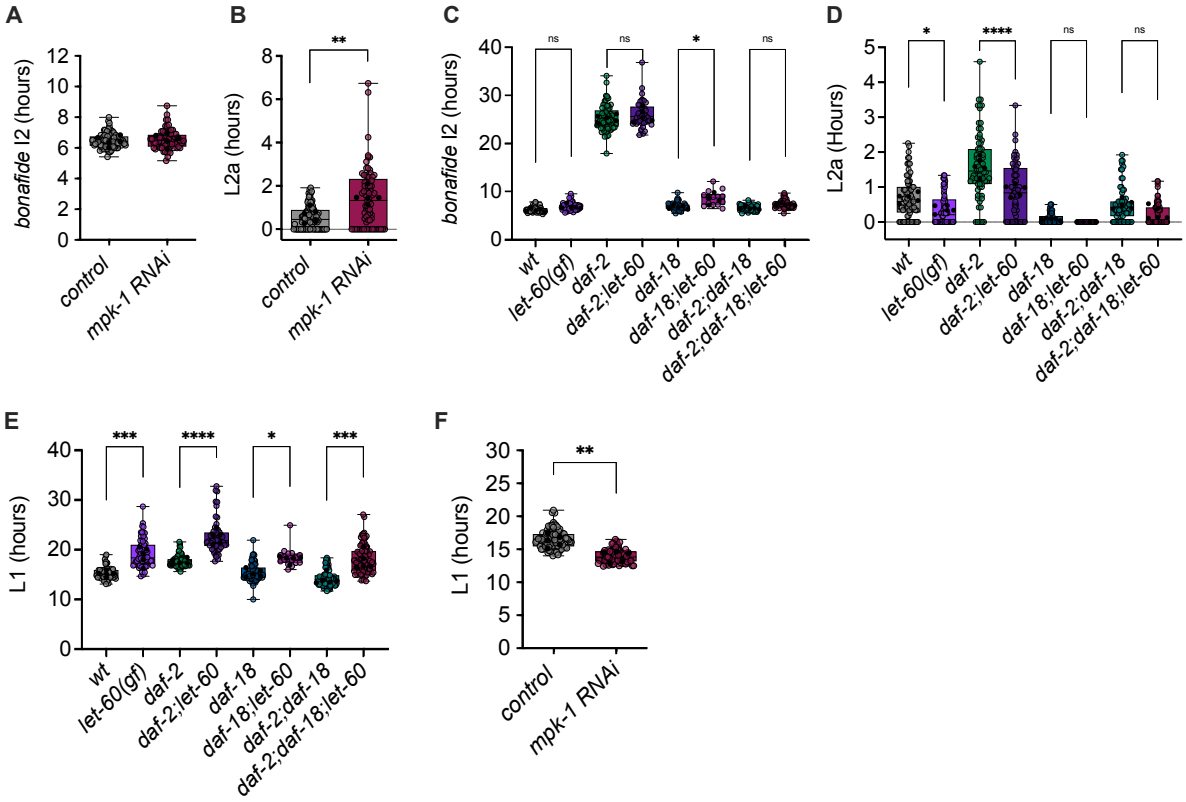

Figure 4. RAS signaling modulates transient larval arrest. (A, B) Duration of the second intermolt (A) and L2a (B) for the wild-type strain, under control and *mpk-1* RNAi treatment, from 5 independent experiments. We performed unpaired t-test with the experimental averages, ** p<0.01. **(C, D)** Duration of the second intermolt (C) and L2a (D) for the wild-type strain, the mutants *daf-2*, *daf-16*, *daf-18*, and *let-60(gf)*, and the corresponding double and triple mutants at 22.5 ºC, in 5 independent experiments. We performed One-way ANOVA followed by Tukey´s multiple comparisons to test differences between all strains. Only comparissons to test the effect of *let-60(gf)* are shown and are marked as ns (not significant), * p<0.05, and **** p<0.0001. **(E)** Duration of the first larval stage (L1) in the wild type, the mutants *let-60(gf)*, *daf-2*, *daf-18*, and the corresponding double and triple mutants. We performed One-way ANOVA followed by Tukey´s multiple comparisons to test differences between all strains. Only the effect of *let-60(gf)* is shown and is marked as * p<0.05, ***p<0.001, **** p<0.0001. **(F)** Duration of L1 for the wild-type strain, under control and *mpk-1* RNAi treatment, from 5 independent experiments. We performed unpaired t-test with the experimental averages, ** p<0.01. Complete report of replicates and statistics results is shown in Table S2 and File S1. Colored or grey circles show values for individual larvae and black dots show the average of each experiment.

daf-2 increases desynchrony between the molting and the developmental timers

To test our hypothesis, we investigated the two timers in parallel, and analyzed the impact of IIS and RAS on each timer. We have defined the precise timing of the transient arrest. It coincides with ecdysis. A relevant process that occurs around ecdysis is seam cell division. Seam cells divide asymmetrically at the beginning of each larval stage, and show an additional symmetric division at the L2 stage, prior to the asymmetric one (*1*). Specifically, we decided to investigate in detail the duration of the two timers from hatching to the second larval stage. We performed time-lapse microscopy of single larvae concealed in 275x275x30 μm hydrogel microchambers (*26*). This setup allows direct observation of hatching and ecdysis as markers of the molting timer. Using strains with the reporter *matIs38,* seam cell divisions of the V lineage were monitored as markers of the developmental timer. Specifically, we measured the timing of the first two seam cell divisions, hatching and the first ecdysis (Fig. 5A). For each of the timers we analyzed the two markers in the wild type, the *daf-2(e1370)* mutant, and the double mutant *daf-2;daf-18*. The first seam cell division (div 1) took place at a similar time relative to hatching for the wild type and *daf-2* but the following event, ecdysis 1, was delayed in the *daf-2* mutant (Fig. 5B). In the wild type, the second seam cell division (div 2) occurred mostly around ecdysis for V1-V4, but V6 usually divides after ecdysis. Div 2 is also delayed in the *daf-2* mutant, but to a larger extent than ecdysis 1. Specifically, the *daf-2(e1370)* mutation delays the time between hatching and the first ecdysis (molting timer) by around 17% (Fig. S4A), while the interval between seam cell divisions (developmental timers) is delayed by 37% in this mutant (Fig. S4B). The differential impact of the *daf-2* mutation on the different timers creates relative desynchronization between ecdysis 1 and div 2 (Fig. 5C). The *daf-18* mutation accelerated all the events, even when compared to the wild type (Fig. 5B, S4A). In the *daf-2;daf-18* most divisions occur before ecdysis (Fig. 5B,C). These results show that reduced insulin signaling impacts the two timers differently, leading to a desynchronization between them. This desynchronization occurs around the transition from L1 to L2, the moment when L2a takes place.

Signaling from DAF-2, which is modulated by DAF-18, converges on the transcription factor DAF-16/FOXO, which is necessary for cell arrest upon nutrient removal during development (*27*). We investigated whether DAF-16 also plays a role in delayed cell division of the *daf-2* mutants in food replete conditions. We assessed activation of DAF-16 by quantifying the subcellular localization of DAF-16::GFP in the wild-type and *daf-2* mutant backgrounds around the first molt. While the wild-type background showed mainly cytoplasmic localization of DAF-16, the *daf-2(e1370)* mutant showed intermediate/nuclear localization, even at this early stage of development and at 20 ºC (Fig. S4C). To link DAF-16 activation in *daf-2* to delayed seam cell division in fed conditions, we performed time-lapse experiments with *daf-2* and *daf-2;daf-16* mutants. The *daf-16* mutation accelerates seam cell divisions of the *daf-2* mutant, but the last divisions (V6 lineage) of the *daf-2;daf-16* occur after ecdysis for 56% of the larvae (Fig. S4D). This is consistent with the partial suppression of the L2a phenotype of *daf-2(e1370)* by the mutation in *daf-16*. In summary, these results support the connection between the transient arrest and the state of synchrony between the molting and the developmental timer.

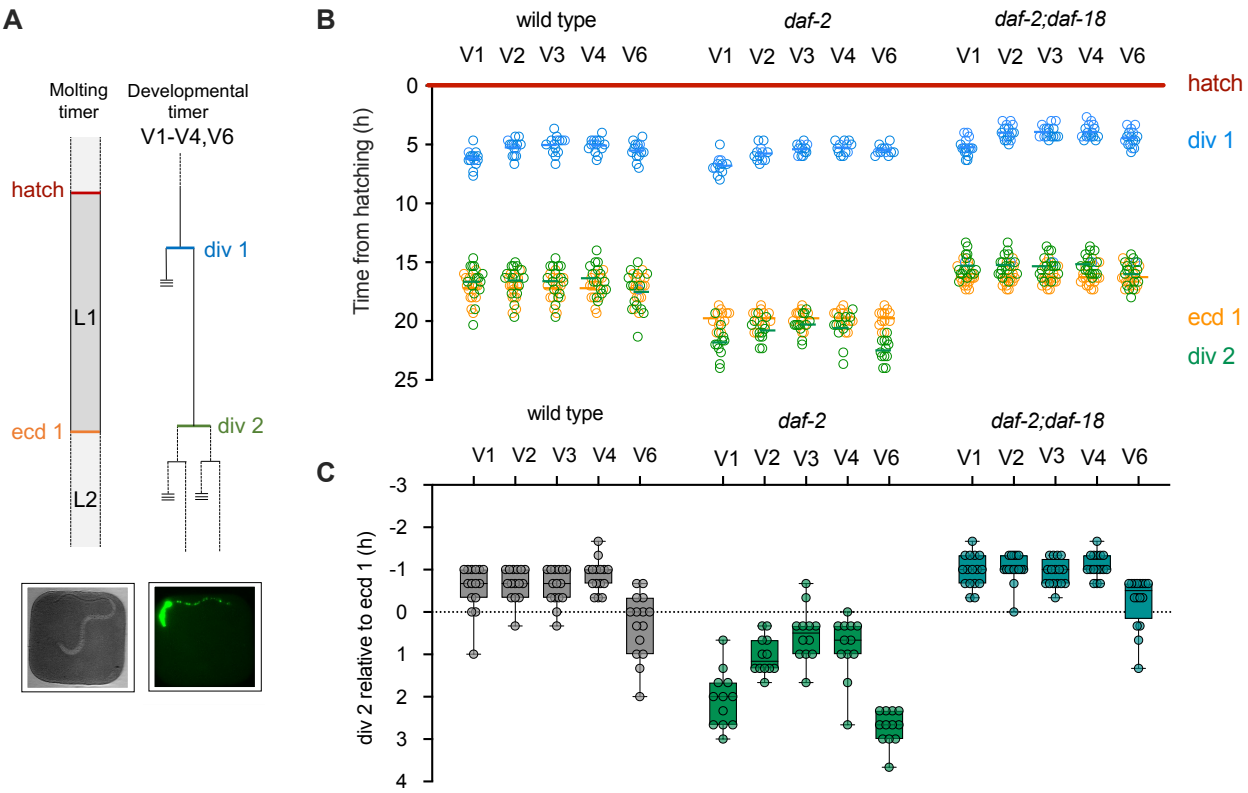

Figure 5. Reduced insulin signaling impacts the two timers differently. (A) Diagram of the events of the molting timer and the developmental timer during the first larval stage. For seam cell division timing we consider the initiation of divisions. **(B)** Timing of the different developmental events div 1, ecd 1 and dev 2 relative to hatching, for each of the seam cells V1-V4, V6. **(C)** Timing of seam cell division (div 2) relative to ecd 1 for the wild type, the *daf-2* mutant and the double mutant *daf-2;daf-18*. Colored or grey circles show values for individual larvae. Complete report of replicates is shown in Table S2.

Desynchrony between timers leads to transient arrest

To link the two processes observed in the *daf-2* mutants, long transient arrest and extended desynchrony between cell divisions and molting, we investigated the state of seam cells during L2a. We combined the reporter used for quantification of development by luminometry with a reporter for seam cell division (*matIs38*). We then initiated development of *daf-2* mutants in a luminometer, followed the luminescence profile in real time until the end of the first molt, and collected larvae from three groups. The first group showed a luminometry profile corresponding to the L2a, with decreasing signal after ecdysis. The second group showed a profile corresponding to a regular intermolt, in this case I2, as determined by a stable, high signal after ecdysis. The third group showed a profile corresponding to a regular intermolt after a period of L2a (Fig. 6A). We then scored the division of seam cells V1-V4 and V6. The L2a group showed a significantly lower fraction of larvae with divided seam cells than the I2 groups, regardless of whether they had previously passed through L2a (Fig. 6A). This result suggests that transient arrest (L2a) could indeed be a consequence of the desynchrony between the molting and cell division timers. To test this hypothesis, we modified the two timers independently and observe the impact on L2a. We expected that delaying specifically the molting timer would reduce L2a, while delaying the developmental timer would increase it. One intervention that increases the duration of the molting timer is caloric restriction (*6*). The ecdysis before L2a is that corresponding to the first larval stage (L1), which includes the first intermolt (I1) and the first molt (M1). We reanalyzed our previous

data to quantify L2a duration for wild-type and *daf-2* larvae under *ad libitum* (AL: 10 g/l *E. coli* OP50-1) and caloric restricted conditions (CR: 0.31 g/l *E. coli* OP50-1) (*6*). Caloric restriction provokes an extension of the L1 by 18 % in the wild type and 36 % in the *daf-2* mutant (Fig. 6B). The increased L1 is accompanied by a reduction of L2a in both the wild-type strain and the *daf-2* mutant (Fig. 6C).

We also tried to delay the cell divisions of the developmental timer by treating developing larvae with Hydroxyurea (HU), which prevents DNA synthesis by replication fork arrest. Since the delay in divisions could also feedback to the molting timer, we aimed for concentrations of Hydroxyurea that allowed complete development and did not increase the duration of the first larval stage. Hydroxyurea at 4 and 8 mM allowed progression through postembryonic development (Fig. S5A), concentration permitted developmental progression without significant delay of the first larval stage (Fig. 6D, Fig. S5B). To confirm the impact of HU on the developmental timer, we analyzed the state of seam cell division of the larvae treated with 4 mM HU at the timing of ecdysis. To increase the number of analyzed larvae and therefore increase the precision of the measurement, we used populations of synchronous larvae. When collected at the average time of ecdysis according to the luminometry data (Fig. S5C), the sample exposed to 4 mM Hydroxyurea showed a significant increase in the fraction of larvae without seam cell divisions (Fig. S5D), confirming that the treatment with HU increases the desynchrony between timers. Indeed, at 4 mM Hydroxyurea the L2a was significantly prolonged compared to the control condition (Fig. 6E). These results show that the relative desynchrony between the two timers determines the duration of L2a.

Finally, we asked whether increased transient arrest is a general principle for other interventions that affect the duration of development. *C. elegans* development shows a strong temperature dependence (*28*). We focused on this environmental cue as, despite the slowed developmental rate at lower temperature, the events of cell divisions and ecdysis occurred at the same time relative to the duration of the total development (*5*). This means that reduction of speed due to temperature does not involve increased desynchrony between ecdysis and cell divisions. Since we previously characterized the regulation by temperature of postembryonic development for temperature between 10 and 27 ºC (*6*), we could extract information about transient arrest from this dataset. The duration of the L1 stage was about 17 hours at 20 ºC, but increased to 26 hours at 16 ºC and to 50 hours at 12 ºC. At 22 ºC, the duration of L1 decreases to approximately 15 hours (Fig. 6F). Despite the change in developmental rate, L2a showed similar values at all temperatures tested (Fig. 6G). This means that the developmental timer is not *per se* more susceptible to environmental interventions that reduce developmental rate and consequently, increased transient arrest is neither a trivial nor a direct consequence of slow development.

Taken together, our results support the idea that the molting timer can pause after ecdysis to allow other developmental events in that module to complete before initiation of the following larval stage. As we have observed, the alteration in the order of developmental events is tolerated by the system and is not solved by pausing the molting timer. However, such a mechanism prevents that desynchrony provoked by a delayed timer amplifies over the course of development.

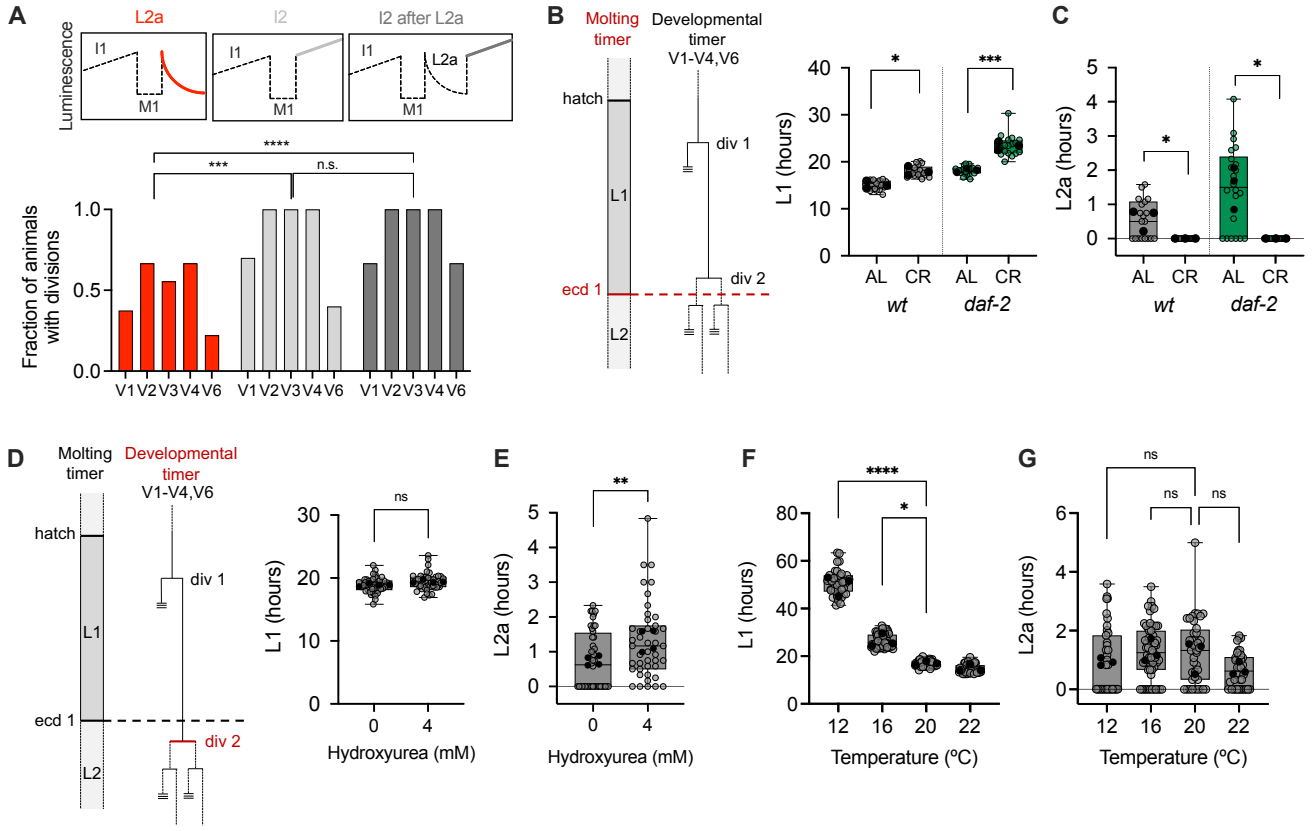

Figure 6. Independent modification of the timers alters the duration of L2a. (A) Diagram showing the moment of collection of the three categories of larva according to their luminometry profile (top) and fraction of animal showing divided seam cells (V1-V4, V6) for each of the three categories (bottom). The fraction of animals was calculated from 9 larvae in L2a, 10 larvae in I2, and 9 larvae in I2 after L2a. We performed two-way ANOVA followed by Tukey´s multiple comparison to assess the effect of the group across all cells analyzed. **(B-C)** Experimental design and duration of L1 (B) and L2a (C) for the wild type and the *daf-2(e1370)* mutant in *ad libitum* (AL) and calorie restricted (CR) larvae, in three independent experiments. For each strain, we performed a t-test to evaluate the effect of the feeding regime. **(D-E)** Experimental design and duration of L1 (D) and L2a (E) for larvae treated with 4 mM Hydroxyurea, and without treatment, in four independent experiments. We performed One-way ANOVA followed by Dunnet´s multiple comparisons to test differences between each of the treatments and the untreated larvae. Colored and grey circles show values for individual larvae and black dots show the average of each experiment. **(F-G)** Duration of the L1 (F) and L2a (G) at 12, 16, 20 and 22 ºC in three independent experiments. We performed One-way ANOVA followed by Tukey´s multiple comparisons to test differences between all strains. Only the differences compared to 20 ºC are shown. Colored or grey circles show values for individual larvae and black dots show the average of each experiment. Complete report of replicates and statistics results is shown in Table S2 and File S1. Statistically significant differences are marked as * $p<0.05$, ** $p<0.01$, ***$p<0.001$, **** $p<0.0001$.

DISCUSSION

Identification of transient arrest

The postembryonic development of *C. elegans* is composed by four larval stages that proceed in a seemingly continuous manner when animals grow in favorable conditions. Different events of developmental arrest have been identified in response to starvation, but these are reversed only when environmental conditions change. The identification of transient life states performed by morphological studies is unlikely, as not all states may be visually identifiable. Since these types of processes may also be highly variable, performing individual analysis with large numbers of larvae (e.g. high throughput) is the key to discovering features of development that deviate from average timing. Using a method for continuous monitoring of *C. elegans* development, we have identified a state of arrest of the molting timer in fed conditions (Fig. 1), that due to its variable and transient nature would be difficult to unveil by other methods. When developmental processes are controlled by different timers, the synchronization between them is necessary to maintain the correct order of the events. The presence of this arrest means that, even in the wild type background and in replete conditions, there is a brake on developmental progression, that could represent a mechanism to accommodate resynchronization between timers.

Regulation by sensing pathways

Transient larval arrest is more frequent and lasts longer in *daf-2* mutants, but this phenotype is independent of other developmental phenotypes of the mutant. We have shown this in several ways. First, the duration of the second intermolt and that of L2a is not consistently proportional in different Class 1 *daf-2* alleles, and selective degradation of DAF-2 leads to increases in the duration of the second intermolt but does not increase L2a (Fig. 2A,B,E,F). Second, the *daf-16* and *daf-18* mutations completely suppress the extended duration of intermolts but not the increase duration of L2a (Fig. 3B,C,F,G). Third, *mpk-1* knockdown increases and *let-60(gf)* reduces L2a without showing any impact on the duration of the second intermolt. These results imply that transient larval arrest emerges as a result of a process or processes that convey information from at least two major signaling pathways. Several studies have tried to make the connection between IIS (including DAF-18/PTEN) and RAS signaling in *C. elegans* (*16*, *23*, *24*, *29*). However, we have shown that transient arrest represents a complex phenotype that arises from the relationship between two different processes, molting and cell divisions. While we attempted to use epistasis to investigate the connection between IIS and RAS in the control of transient larval arrest, it is plausible that the interactions observed are only due to the relative impact of each of the pathways on the molting timer and/or the developmental timer independently. Unbalanced impact on these two processes results in variation of the duration of L2a. This could apply to other phenotypes used to investigate this or other genetic interactions, if those phenotypes reflect distinct impact on the two developmental timers.

Timer desynchrony

Indeed, the possibility that IIS and RAS might impact more than one process to determine transient arrest led us to investigate the progression of the developmental timer. We observed that seam cell divisions are more sensitive than the molting program to reduced insulin signaling (Fig. S4A-C). Insulin signaling independently impacts the two timers acting on *C. elegans* development, the molting timer, and the developmental timer. Reduced insulin signaling reduces the speed of both timers but to different extents, leading to a delay on seam cell division relative to ecdysis (Fig. 5C), that is, a desynchronization between the timers. This feature is related to the

transient arrest of the molting timer (L2a), as *daf-2* larvae that are in L2a are more likely to have undivided seam cells than those that are at the beginning of the second intermolt (Fig. 6A). These results suggest that the transient arrest of the molting timer that we observe as L2a could represent a mechanism to buffer the delay in seam cell divisions and allow resynchronization between the two timers. Delay of cell divisions and differentiation during the L2 stage by the nicotinic agonist 1,1-dimethyl-4-phenylpiperazinium (DMPP), which does not affect the molting timer, leads to exposure of a defective L3 cuticle to the environment and provokes death of the larva (*4*). This suggests that an accumulated delay of the developmental timer leads to larval death, pointing to the necessity of programmed mechanisms that allow resynchronization in normal development. *Drosophila melanogaster* presents a well characterized example of using checkpoints to coordinate the growth of individual tissues. If imaginal discs, which contain the developing organs of the adult, are damaged or present abnormal growth, the insulin like peptide DILP8 is secreted. This peptide activates a systemic neuroendocrine circuit that suppresses the production of ecdysone, the hormone that triggers pupariation, delaying metamorphosis and the emergence of the adult fly (*30*, *31*). Similarly, the transient arrest of the molting timer after the first molt observed in our work delays the initiation of the L2 stage, allowing delayed developmental events to catch up.

Not all interventions that delay development increase transient arrest. The temperature dependence of development in *C. elegans* follows the Arrhenius equation, which describes the relationship between temperature and the rate of first-order chemical reactions (*6*). This intervention if therefore fundamentally different to reduced insulin signaling, since it likely involves a change in the speed of chemical reactions rather than in cellular signaling. Unlike reduced insulin signaling, temperature modulates larval development by temporal scaling of developmental events. At temperatures between 15 and 23 ºC, cell divisions and ecdysis occur at the same times relative to the duration of development (*5*). With this previous information, we predicted that temperature should not impact transient arrest. Indeed, L2a is similar at temperatures between 12 and 22 ºC.

Modularity of *C. elegans* development

Our investigation of the transient larval arrest offers other insights about *C. elegans* developmental timing. The transient arrest occurs at the beginning of larval stages, the same moment when a nutritional checkpoint was previously observed. Starvation can lead to developmental arrest at different stages. If embryos hatch in the absence of food, the newly hatched larvae arrest at the first larval stage L1 (*32*, *33*). Starvation during L2 and L3 also leads to developmental arrest at the beginning of the following larval stage, L3 and L4 respectively (*27*). When larvae are deprived of food midway through a larval stage, they continue development only until the beginning of the next stage, e.g. a nutritional checkpoint. Transient larval arrest could respond to a delay to pass the nutritional checkpoints previously described for L3 and L4, and that have also been proposed to exist at the beginning of L2. Indeed, fed *daf-2(e1370)* mutants grown to mid-L2 at 15 ºC and then shifted to 25 ºC, paused preferentially early in the L3 and L4 stages (*27*, *34*). Transient arrest also coincides with the phase of arrest of developmental oscillations in gene expression (*35*). Finding that the molting timer arrests at the nutritional checkpoints because of timer desynchrony highlights the modular nature of *C. elegans* development, and points to the presence of a mechanism to control that a developmental module is completed before the initiation of the following larval stage.

Materials and Methods

C. elegans maintenance and strains

C. elegans strains were cultured following standard methods (*36*). Animals were grown and maintained on nematode growth media (NGM) with a lawn of *Escherichia coli* OP50-1 at 20 °C. As an exception, for the experiments corresponding to figures 2C-D, 3D-E, and S2A-D, the strains were maintained at 16.5 °C prior to the experiments, since the *daf-2(e979)* mutant forms dauers at 20 ºC. All strains used are listed in Table S1.

Bacterial strains

For maintenance plates and experiments the food source was *E. coli* OP50-1. The only exception is Fig. 4A,B and F, where we used *E. coli* HT115 for the RNAi treatment, as listed in the Table S1.

Luminometry of single worms

To analyse the developmental timing of single worms we used the bioluminescence-based method previously described (*11*). To obtain age-synchronized eggs, 10-15 hermaphrodites were transferred to a fresh NGM plate, allowing them to lay eggs for one hour. For experiments with six conditions or less, synchronized-eggs were individually placed in wells of a 96 well-plate containing 100 µl of S-basal (5 µg/ml cholesterol) with 200 µM Luciferin. After placing all embryos, 100 µl of S-basal with 20 g/l *E. coli* OP50-1 was added to each well. For experiments with more than 6 conditions, the eggs were placed individually in wells of a 384-well plate containing 25 µl of S-basal (5 µg/ml cholesterol) with 400 µM Luciferin, adding 25 of S-basal with 20 g/l *E. coli* OP50-1 per well after all eggs were transferred. In both cases, samples from different strains or conditions were alternated to avoid local effects. Plates were sealed with a gas-permeable membrane and placed in a luminometry reader (Berthold Centro XS3) localized inside a cooled incubator (Panasonic MIR-254). Luminescence was recorded for 1 s (for 96-well plate) or 0.7 s (for 384-well plate) at 5-min intervals until reaching adulthood.

DAF-2 auxin-mediated degradation

We investigated the effect of DAF-2 auxin-mediated degradation on development using a strain carrying daf-2 endogenously tagged with a degron (*hq363[daf-2::degron::mNeonGreen*]) and a single copy transgene to express TIR1 in all somatic tissues *ieSi57 [eft-3p::TIR1::mRuby::unc-54 3' UTR + Cbr-unc-119(+)] II.* To induce degradation, we used the auxin analogue 1-Naphthaleneacetic acid, added to the S-basal used for the luminometry plates at the indicated concentrations.

RNAi treatment

We performed RNAi knockdown by feeding for *mpk-1*. We analysed the RNAi treatment in the second generation to increase the efficiency of the treatment. The first generation was cultured from L4 stage during one day in NGM plates lawn with control or RNAi bacteria. To prepare the plates, we placed 200 µl of RNAi or control bacterial cultures grown overnight on NGM plates with 1 mM IPTG and 100 µg/ml Ampicillin. After the bacterial lawn had dried out, the plates were incubated for 5 h at 37 °C. The day prior to the experiment, 10-15 L4 hermaphrodite larvae were transferred to RNAi or control bacteria NGM plates to let them reach the adulthood stage. After 24 hours, gravid adults were moved to fresh NGM and were allowed to lay eggs from one hour approximately. We measured the development of these worms as described above, with the difference that age-synchronized embryos were transferred to wells containing 100 µl of S-basal (5 µg/ml cholesterol) with 200 µM Luciferin, 2 mM IPTG and 200 µg/ml Ampicillin. To provide the

food source after placing all embryos, we added 100 µl of S-Basal containing 20 g/l of the control or the RNAi bacteria to each well.

Live imaging of single worms

To study the development and seam cells divisions of single worms we adapted a system for time-lapse microscopy in (*26*). To prepare the acrylamide-gel chambers, we used silicon master moulds with microchambers dimensions of 275x275x30 µm. The microchambers were prepared by first mixing a polyacrylamide solution containing 10 % acrylamide/bis-acrylamide (29:1), 1 % ammonium persulfate and 0.1 % TEMED. The liquid solution was pipetted into a compartment composed by the master mould glued to a methacrylate frame. After filling all the compartment, a glass microscope slide was placed on top to seal the compartment and let it to solidify for 0.5-2 hours. The resulting polyacrylamide gel is washed with ddH_2O at least 4 times and stored in ddH_2O.

To perform the experiments, the polyacrylamide microchamber used is previously stabilized in M9 during 1 hour prior to the experiment. To prepare the long-term imaging, a methacrylate frame is sticked to a microscope slide. The M9-stabilized microchamber is then placed on top of the slide, within the frame. To place embryos in the polyacrylamide chambers we proceeded as previously described (*37*). We obtained age-synchronized embryos by transferring 10-15 gravid hermaphrodites to fresh NGM plates and letting them to lay eggs for one hour. Using an eyelash, eggs were individually transferred to the wells of the microchamber (1 egg per well). After eggs were transferred, we collected some OP50-1 from NGM plates using the eyelash and added it to wells as food source. The compartment was filled with M9 and sealed with cover slides.

We performed the time-lapse imaging in a Leica scope M205 FCA with a motorized stage, using GFP excitation/emission filters. Time-lapse was performed by taking pictures every 20 minutes for each worm in a Z-stack of 40 µm divided in 11 steps. Worms were photographed in two different channels (white light channel and GFP channel) with exposure times of 50 ms for both cases. The developing larvae worms were recorded for approximately 40 hours. For figure S4D, we used strains that contains the reporter *sevIs1* in addition to *matIs38.* Since *sevIs1* expresses GFP ubiquitously, we visualized seam cells using the RFP signal from *matIs38.* For this experiment we used the Leica M205 FCA scope and a Nikon Eclipse Ti2 microscope.

Seam cell division analysis at specific larval stages

We analysed the state of seam cell division specific developmental stages. To do so, we perform the luminometry assay as described above (see "*Luminometry of single worms*") using worms combining the bioluminescence (*sevIs1*) and the seam cell fluorescence-tagged reporter (*matIs38*). After approximately 24 hours of initiating, we monitored the larval developmental progress continuously. When larvae were transitioning through the stage of interest, the specific worms were taken independently from the plate by pipetting the entire content of the well. Individual worms were isolated and washed from food M9. Finally, worms were immobilized using 10 mM Levamisol diluted in M9 and placed in agarose pads. Larvae with seam cell divisions were identified using a Leica scope M205 FCA and RFP excitation/emission filters.

Seam cell division analysis after ecdysis in populations

Before the experiment, we precisely timed the moment of ecdysis in each of the conditions tested using the method described above (Luminometry of single worms), this time, starting with L1 arrest larvae. We obtained embryos by treatment of gravid adults with an alkaline hypochlorite solution. We adjusted the concentration to 20 embryos/µl in M9 buffer and incubated them at 20 ºC with

gentle shaking, leading to hatching and arrest at the L1 stage. After 24 hours, we resumed development directly in a luminometer plate, setting the plates as described above. Once we had calculated the average timing of ecdysis, we proceeded to perform the experiments using population of larvae synchronized in the same manner but using 20 larvae per well. We confirmed that the amount of larvae did not impact timing, as we had also shown before (*11*). At the appropriate times for each condition, we collected larvae from the specific wells and counted the fraction of larvae with divisions using a Leica scope M205 FCA and RFP excitation/emission filters.

Hydroxyurea treatment

To test the effect of cell division blocking chemicals on the development, we treated worms with Hydroxyurea (HU) specifically during the postembryonic development. To do so, we performed the luminometry assay as described above (see "*Luminometry of single worms*"). The difference is that eggs were placed in wells containing 90 µl of S-basal (5 µg/ml cholesterol) with 200 µM Luciferin and after placing them, we added 90 µl of S-basal with 20 g/l *E. coli* OP50-1 to each well, so the final volume is 180 µl per well. 12 hours after the beginning of the luminometry recording, the plate was unloaded from the luminometer. For non-treated, we added 20 µl ddH_2O per well. For the 4 mM HU treatment, 40 µl of the 1 M HU stock was diluted in 960 µl ddH_2O and 20 µl of that mix was added to each well. For the 8 mM HU treatment, 80 µl of the 1 M HU stock was diluted in 920 µl ddH_2O and 20 µl of that mix was added to each well. After adding the HU, the plate was sealed with a new gas-permeable membrane and placed again in a luminometry reader.

Statistical analysis

For statistics we have used the averages of independent biological replicates to avoid the inflated N value from using individual animals. Before calculating the averages, we applied a filter for outliers using ROUT (Q=0.2%) on Graphpad Prism 10. The number of larvae and number of independent replicates performed are shown in Table S2. For the data on Fig. 1E we used two-way ANOVA to test both the effects of genotype and larval stage, followed by Fisher´s LSD to reveal significant differences between genotypes at each stage. For the data on Fig. 6A we used two-way ANOVA followed by Tukey´s multiple comparison to test significant differences between groups of larvae, considering the global state of all seam cells tested. We used unpaired two-tailed t-test to compare the means of two groups in Fig. 4A,B,F, Fig. S3C-E, Fig. 6B,C, and Fig. S5D. For the rest of the experiments, we used one-way ANOVA to compare more than two groups. After one-way ANOVA, we either perform Dunnett´s multiple comparison to compare the average of each genotype/condition to the average of the wild type, or Tukey´s multiple comparison to compare the average of each genotype to all the other genotypes. For clarity, some plots show only relevant comparisons but all the results from statistical testing are shown in File S1. In all cases, * means $p>0.05$, ** $p>0.01$, *** $p>0.001$, and **** $p>0.0001$. Graphs and statistics were performed on Graphpad Prism 10.

Acknowledgments

Some strains were provided by the *Caenorhabditis* Genetics Center (CGC), which is funded by NIH Office of Research Infrastructure Programs (P40 OD010440). Fig. 3A was created with BioRender.com.

Funding:
Work in the Olmedo lab is supported by the grants PID2022-139009OB-I00 funded by MICIU/AEI/ 10.13039/501100011033 and by "ERDF A way of making Europe", and P20-RT-01248 (PAIDI2020, Proyecto cofinanciado por fondos del Programa Operativo FEDER Andalucía 2014-2020 y por la Consejería de Transformación Económica, Industria, Conocimiento y Universidades de la Junta de Andalucía). Initial observations of *daf-2* delayed divisions were performed by M.O. at the lab of J.v.Z during a COST GENiE Short Term Scientific Mission granted to M.O. (COST-STSM-BM1408-35915). FJRE was supported by a contract of the VPPI-University of Sevilla (Contratos de Personal Investigador en Formación), and a FEBS short-term fellowship. MMB was supported by a postdoctoral contract from the "Programa de Ayudas a la I+D+i, en Régimen de Concurrencia Competitiva en el Ámbito del Plan Andaluz de Investigación, Desarrollo e Innovación (PAIDI 2020)". AMC was supported by a contract of the VII PPIT- University of Sevilla (Contratos de Acceso al Sistema Español de Ciencia, Tecnología e Innovación). The Nikon Eclipse Ti2 microscope system was funded by DFG (INST 86/1851-1 FUGG).

Author contributions:
Conceptualization: FJRE, AMC, MO
Methodology: FJRE, FS, NG, MM, JvZ, MO
Investigation: FJRE, AMR, MMB, SGG, FRP
Visualization: FJRE, MO
Supervision: AMC, MO
Writing—original draft: FJRE, AMC, MO
Writing—review & editing: FJRE, FS, NG, MM, JvZ, AMC, MO

Competing interests:
Authors declare that they have no competing interests.

Data and materials availability:
All data are available in the main text or the supplementary materials.

References

1. J. E. Sulston, H. R. Horvitz, Post-embryonic cell lineages of the nematode, *Ceanorhabditis elegans*. *Developmental Biology*. **56**, 110–156 (1977).

2. D. M. Raizen *et al.*, Lethargus is a *Caenorhabditis elegans* sleep-like state. *Nature*. **451**, 569–572 (2008).

3. R. N. Singh, J. E. Sulston, Some observations on moulting in *Caenorhabditis elegans*. *Nematologica*. **24**, 63–71 (1978).

4. A.-F. Ruaud, J.-L. Bessereau, Activation of nicotinic receptors uncouples a developmental timer from the molting timer in *C. elegans*. *Development*. **133**, 2211–2222 (2006).

5. O. Filina, B. Demirbas, R. Haagmans, J. S. van Zon, Temporal scaling in *C. elegans* larval development. *Proceedings of the National Academy of Sciences*. **119**, e2123110119 (2022).

6. A. Mata-Cabana *et al.*, Deviations from temporal scaling support a stage-specific regulation for *C. elegans* postembryonic development. *BMC Biol*. **20**, 94–15 (2022).

7. L. T. MacNeil, E. Watson, H. E. Arda, L. J. Zhu, A. J. M. Walhout, Diet-Induced Developmental Acceleration Independent ofTOR and Insulin in *C. elegans*. *Cell*. **153**, 240–252 (2013).

8. A. F. Ruaud, I. Katic, J. L. Bessereau, Insulin/Insulin-Like Growth Factor Signaling Controls Non-Dauer Developmental Speed in the Nematode *Caenorhabditis elegans*. *Genetics*. **187**, 337–343 (2011).

9. C. T. Murphy, Insulin/insulin-like growth factor signaling in *C. elegans*. *WormBook*, 1–43 (2013).

10. M. Ebisuya, J. Briscoe, What does time mean in development? *Development*. **145** (2018), doi:10.1242/dev.164368.

11. M. Olmedo, M. Geibel, M. Artal-Sanz, M. Merrow, A High-Throughput Method for the Analysis of Larval Developmental Phenotypes in *Caenorhabditis elegans*. *Genetics*. **201**, 443–448 (2015).

12. M. Olmedo *et al.*, Prolonged quiescence delays somatic stem cell-like divisions in *Caenorhabditis elegans* and is controlled by insulin signaling. *Aging Cell*. **19**, e13085 (2020).

13. C. Azzi, F. Aeschimann, A. Neagu, H. Großhans, A branched heterochronic pathway directs Juvenile-to-adult transition through two LIN-29 isoforms. *eLife*. **9** (2020), doi:10.7554/eLife.53387.

14. J. R. Wet, K. V. Wood, M. DeLuca, D. R. Helinski, S. Subramani, Firefly luciferase gene: structure and expression in mammalian cells. *Molecular and Cellular Biology*. **7**, 725–737 (1987).

15. D. Gems *et al.*, Two Pleiotropic Classes of daf-2 Mutation Affect Larval Arrest, Adult Behavior, Reproduction and Longevity in *Caenorhabditis elegans*. *Genetics*. **150**, 129–155 (1998).

16. M. Nanji, N. A. Hopper, D. Gems, LET-60 RAS modulates effects of insulin/IGF-1 signaling on development and aging in *Caenorhabditis elegans*. *Aging Cell*. **4**, 235–245 (2005).

17. Y.-P. Zhang *et al.*, Intestine-specific removal of DAF-2 nearly doubles lifespan in *Caenorhabditis elegans* with little fitness cost. *Nature Communications*. **13**, 6339–18 (2022).

18. S. Gottlieb, G. Ruvkun, *daf-2*, *daf-16* and *daf-23*: genetically interacting genes controlling Dauer formation in *Caenorhabditis elegans*. *Genetics*. **137**, 107–120 (1994).

19. P. L. Larsen, P. S. Albert, D. L. Riddle, Genes that regulate both development and longevity in *Caenorhabditis elegans*. *Genetics*. **139**, 1567–1583 (1995).

20. P. Bharill, S. Ayyadevara, R. Alla, R. J. Shmookler Reis, Extreme Depletion of PIP3 Accompanies the Increased Life Span and Stress Tolerance of PI3K-null *C. elegans* Mutants. *Front. Genet.* **4**, 34 (2013).

21. V. T. Mihaylova, C. Z. Borland, L. Manjarrez, M. J. Stern, H. Sun, The PTEN tumor suppressor homolog in *Caenorhabditis elegans* regulates longevity and dauer formation in an insulin receptor-like signaling pathway. *Proc. Natl. Acad. Sci. U.S.A.* **96**, 7427–7432 (1999).

22. J. Liu *et al.*, Insulin activates the insulin receptor to downregulate the PTEN tumour suppressor. *Oncogene*. **33**, 3878–3885 (2014).

23. A. L. Lopez III *et al.*, DAF-2 and ERK Couple Nutrient Availability to Meiotic Progression during *Caenorhabditis elegans* Oogenesis. *Developmental Cell*. **27**, 227–240 (2013).

24. I. Nakdimon, M. Walser, E. Fröhli, A. Hajnal, PTEN Negatively Regulates MAPK Signaling during *Caenorhabditis elegans* Vulval Development. *PLoS Genet*. **8**, e1002881–10 (2012).

25. P. Narbonne, P. S. Maddox, J.-C. Labbé, DAF-18/PTEN signals through AAK-1/AMPK to inhibit MPK-1/MAPK in feedback control of germline stem cell proliferation. *PLoS Genet*. **13**, e1006738 (2017).

26. N. Gritti, S. Kienle, O. Filina, J. S. van Zon, Long-term time-lapse microscopy of C. elegans post-embryonic development. *Nature Communications*. **7**, 1–9 (2016).

27. A. J. Schindler, L. R. Baugh, D. R. Sherwood, Identification of Late Larval Stage Developmental Checkpoints in *Caenorhabditis elegans* Regulated by Insulin/IGF and Steroid Hormone Signaling Pathways. *PLoS Genet*. **10**, e1004426 (2014).

28. L. Byerly, R. C. Cassada, R. L. Russell, The Life Cycle of the Nematode *Caenorhabditis elegans.* I. Wild-Type Growth and Reproduction. *Developmental Biology*. **51**, 23–33 (1976).

29. P. Narbonne, P. S. Maddox, J.-C. Labbé, DAF-18/PTEN locally antagonizes insulin signalling to couple germline stem cell proliferation to oocyte needs in *C. elegans*. *Development*. **142**, 4230–4241 (2015).

30. J. Colombani, D. S. Andersen, P. Léopol, Secreted peptide dilp8 coordinates *Drosophila* tissue growth with developmental timing. *Science*. **336**, 582–585 (2012).

31. A. Garelli, A. M. Gontijo, V. Miguela, E. Caparros, M. Dominguez, Imaginal discs secrete insulin-like peptide 8 to mediate plasticity of growth and maturation. *Science*. **336**, 579–582 (2012).

32. T. E. Johnson, D. H. Mitchell, K. Susan, R. Kemal, J. Foy, Arresting development arrests aging in the nematode *Caenorhabditis elegans*. *Mechanisms of Ageing and Development*. **28**, 23–40 (1984).

33. L. R. Baugh, To Grow or Not to Grow: Nutritional Control of Development During *Caenorhabditis elegans* L1 Arrest. *Genetics*. **194**, 539–555 (2013).

34. A. J. Schindler, D. R. Sherwood, Should I stay or should I go? Identification of novel nutritionally regulated developmental checkpoints in *C. elegans*. *worm*. **3**, e979658 (2014).

35. M. W. Meeuse *et al.*, Developmental function and state transitions of a gene expression oscillator in *Caenorhabditis elegans*. *Molecular Systems Biology*. **16**, 1–21 (2020).

36. S. Brenner, The genetics of *Caenorhabditis elegans*. *Genetics*. **77**, 71–94 (1974).

37. H. Bringmann, Agarose hydrogel microcompartments for imaging sleep- and wake-like behavior and nervous system development in *Caenorhabditis elegans* larvae. *Journal of Neuroscience Methods*. **201**, 78–88 (2011).

Supplementary information for:

Desynchronization between timers provokes transient arrest during *C. elegans* development

Short title: Active timer resynchronization during development

Francisco Javier Romero-Expósito[1], Almudena Moreno-Rivero[1], Marta Muñoz-Barrera[1], Sabas García-Sánchez[1], Fernando Rodríguez-Peris[1], Nicola Gritti[2], Francesca Sartor[3], Martha Merrow[3], Jeroen van Zon[2], Alejandro Mata-Cabana[1] and María Olmedo[1,4]

[1] Departamento de Genética, Facultad de Biología, Universidad de Sevilla, Spain.
[2] AMOLF, Amsterdam, The Netherlands.
[3] Institute of Medical Psychology, Faculty of Medicine, LMU Munich, Germany.

[4] Correspondence: mariaolmedo@us.es
Keywords: Insulin, RAS, Proliferation, Arrest, Developmental timers

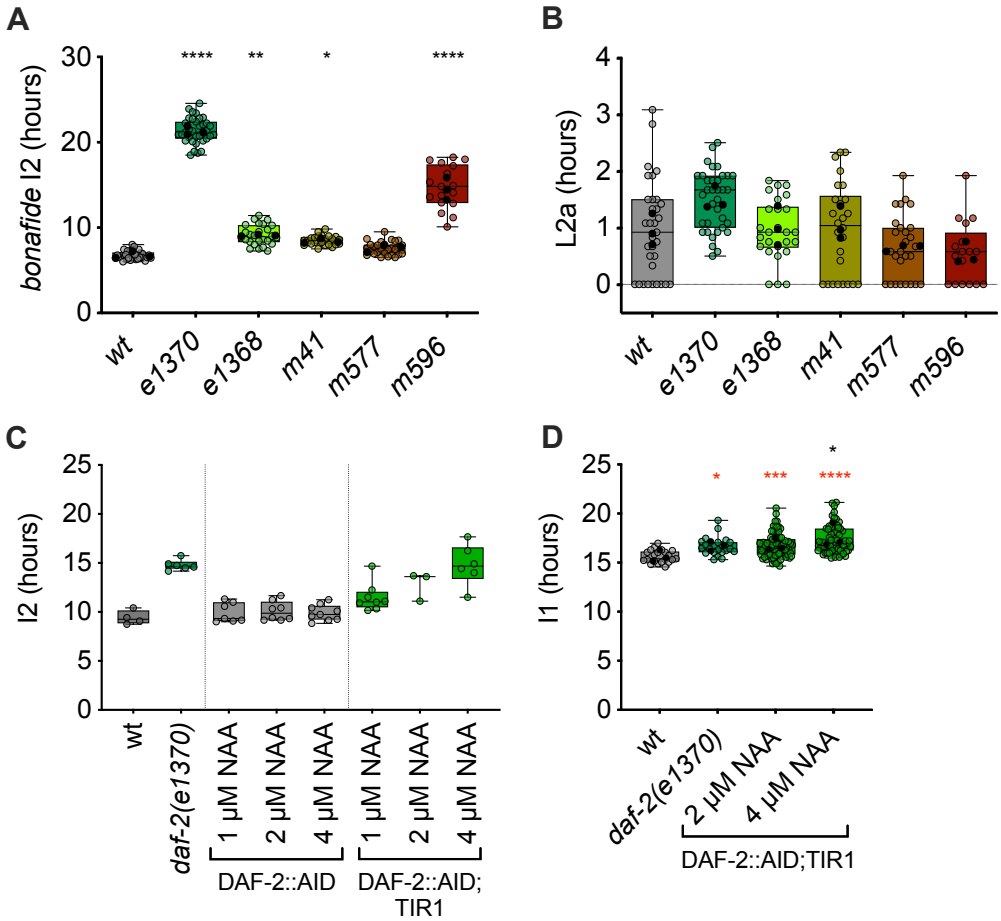

Figure S1. (Related to figure 2). (A, B) Duration of the *bonafide* I2 (A), and L2a (B) at 20 ºC, in the wild-type strain, *daf-2(e1370)*, and the *daf-2* class 1 alleles *e1368*, *m41*, *m577,* and *m596* from three independent experiments. **(C)** Duration of the *bonafide* I2 of the wild-type strain, *daf-2(e1370)*, and a strain containing an AID tagged version of DAF-2 (DAF-2::AID), and a strain containing the same tagged version of DAF-2 and expressing TIR1 under the somatic promoter P*eft-3* (DAF-2::AID,TIR1) in the presence of 2 or 4 µM NAA. **(D)** Duration of the first intermolt (I1) of the wild-type strain, *daf-2(e1370)*, and a strain containing an AID tagged version of DAF-2 and expressing TIR1 under the somatic promoter P*eft-3* (DAF-2::AID,TIR1) in the presence of 2 and 4 µM NAA, in the three independent experiments show in Fig 2E,F. Colored circles show values for individual larvae and black dots show the average of each experiment. For each mutant, we compared the averages per experiment to those of the wild type using One-way ANOVA followed by Dunnet´s multiple comparisons. Only significant differences are shown and are marked as * $p<0.05$, ** $p<0.01$, ***$p<0.001$, **** $p<0.0001$. Stars in red show the results from statistical testing using all larvae independently. Complete statistical analysis is shown in File S1.

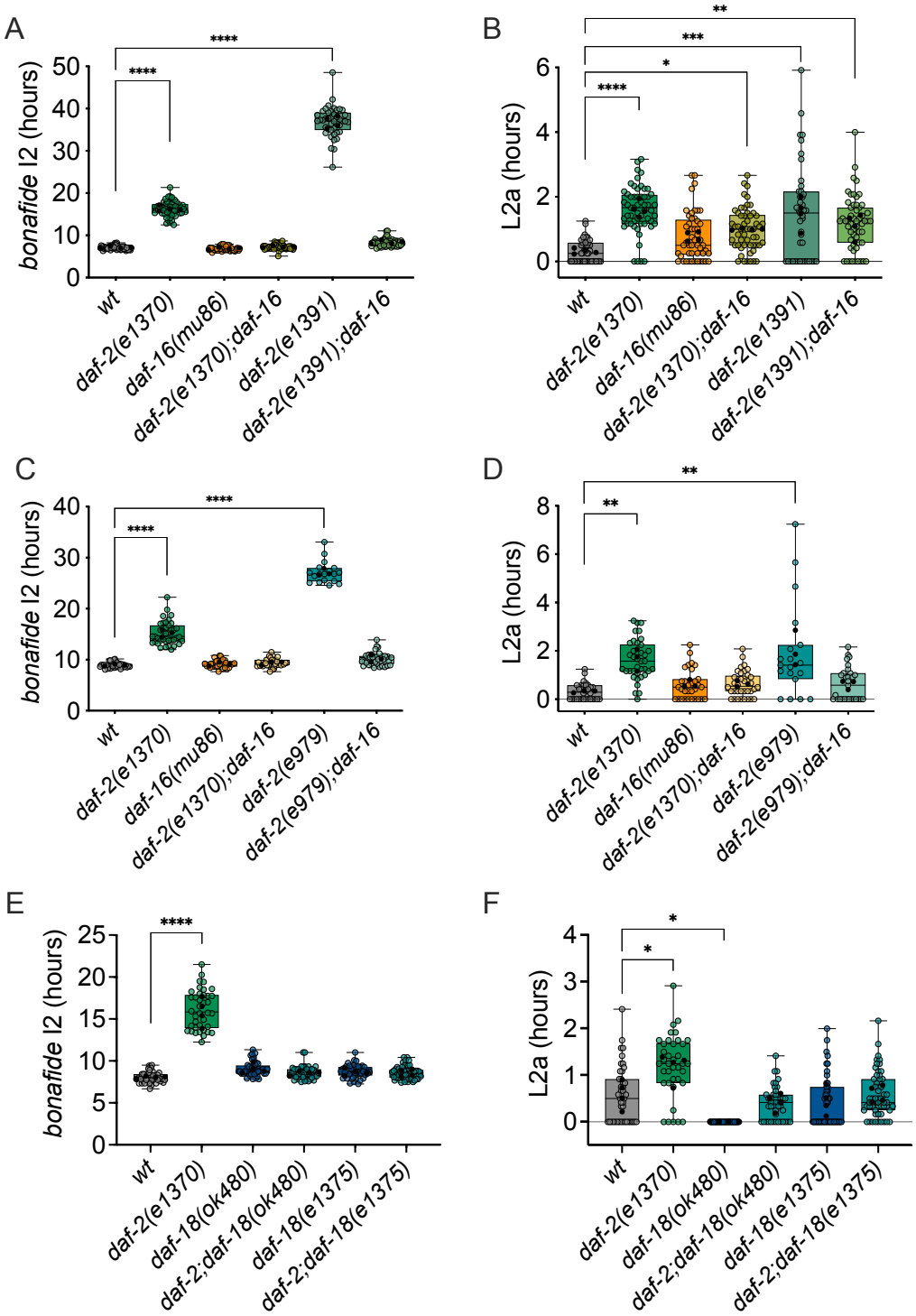

Figure S2. (Related to figure 3). (A, B) Duration of the *bonafide* l2 (A), and L2a (B), in the wild-type strain, *daf-16(mu86)*, *daf-2(e1391)*, and the double mutant *daf-2;daf-16*, from four independent experiments. **(C, D)** Duration of the *bonafide* l2 (C), and L2a (D), in the wild-type strain, *daf-16(mu86)*, *daf-2(e979)*, and the double mutant *daf-2;daf-16*, from three independent experiments. **(E, F)** Duration of the *bonafide* l2 (C), and L2a (D), in the wild-type strain, *daf-2(e1370), daf-18(ok480), daf-18(e1375)*, and the corresponding *daf-2;daf-18* double mutants, from three independent experiments. Colored circles show values for individual larvae and black dots show the average of each experiment. We performed One-way ANOVA followed by Tukey´s multiple comparisons to test differences between all strains. Only significant differences relative to the wild type are shown, and are marked as * $p<0.05$, ** $p<0.01$, ***$p<0.001$, **** $p<0.0001$. Complete statistical analysis is shown in File S1.

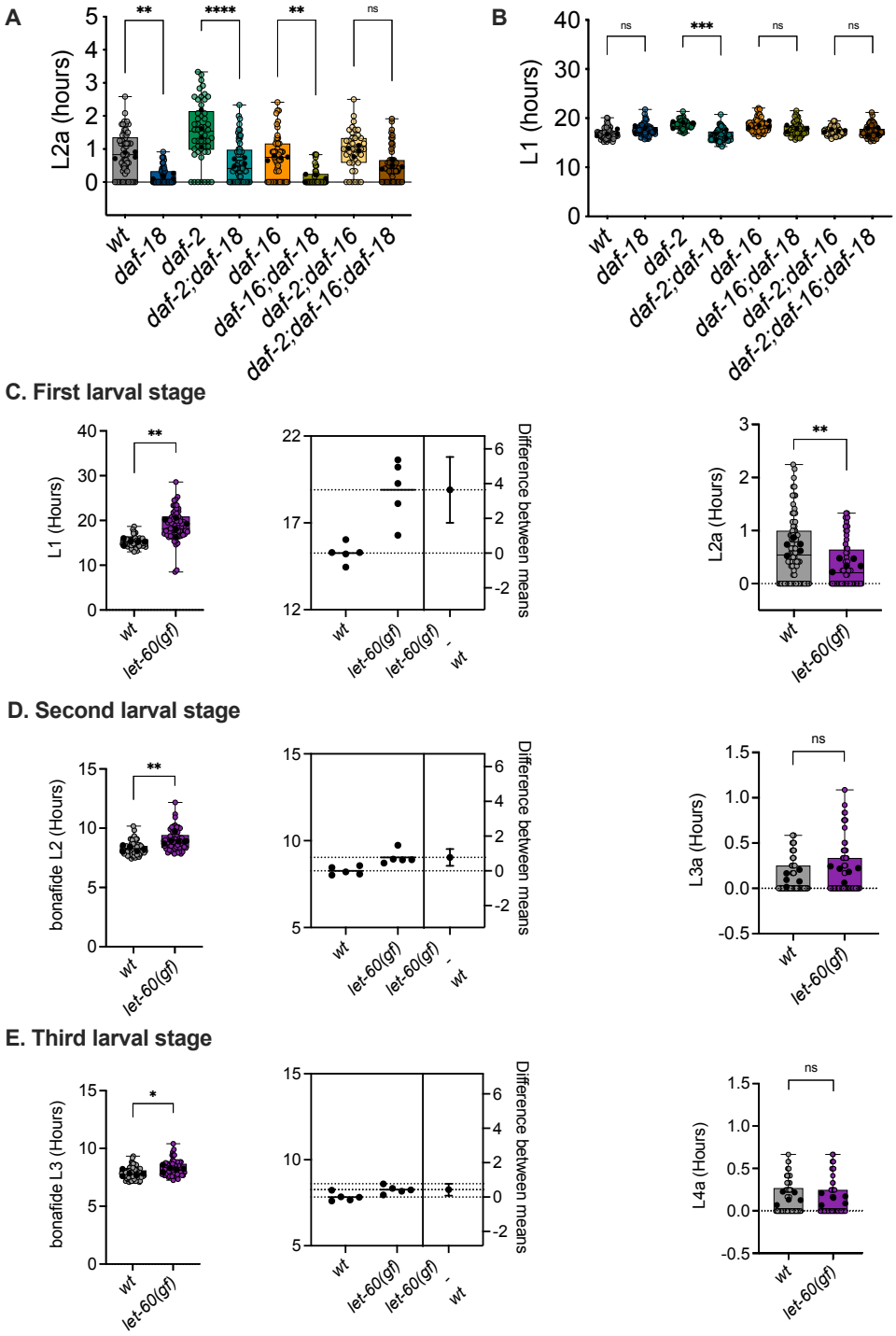

Figure S3. (Related to figure 4). (A) Duration of L2a for the wild type, *daf-2*, *daf-16*, *daf-18*, and the respective double and triple mutants. Replotted from Fig. 3G for clarity. **(B)** Duration of L1 for the wild type and the same mutants as (A). We performed One-way ANOVA followed by Tukey´s multiple comparisons to test differences between all strains. Only the results from comparing the effect of the *let-60(gf)* mutation are shown, and are marked as ns >0.5, and ** p<0.01, ***p<0.001, **** p<0.0001. **(C-E)** Duration of larval stage, difference between means of the larva stage and duration of the subsequent transient arrest for the wild type and the *let-60(gf)* mutant. (C) shows L1 and L2a, (D) shows L2 and L3a and (E) shows L3 and L4a. We performed a t-test to compare means. Grey and colored circles show values for individual larvae, and black dots show the average of each experiment. Complete statistical analysis is shown in File S1.

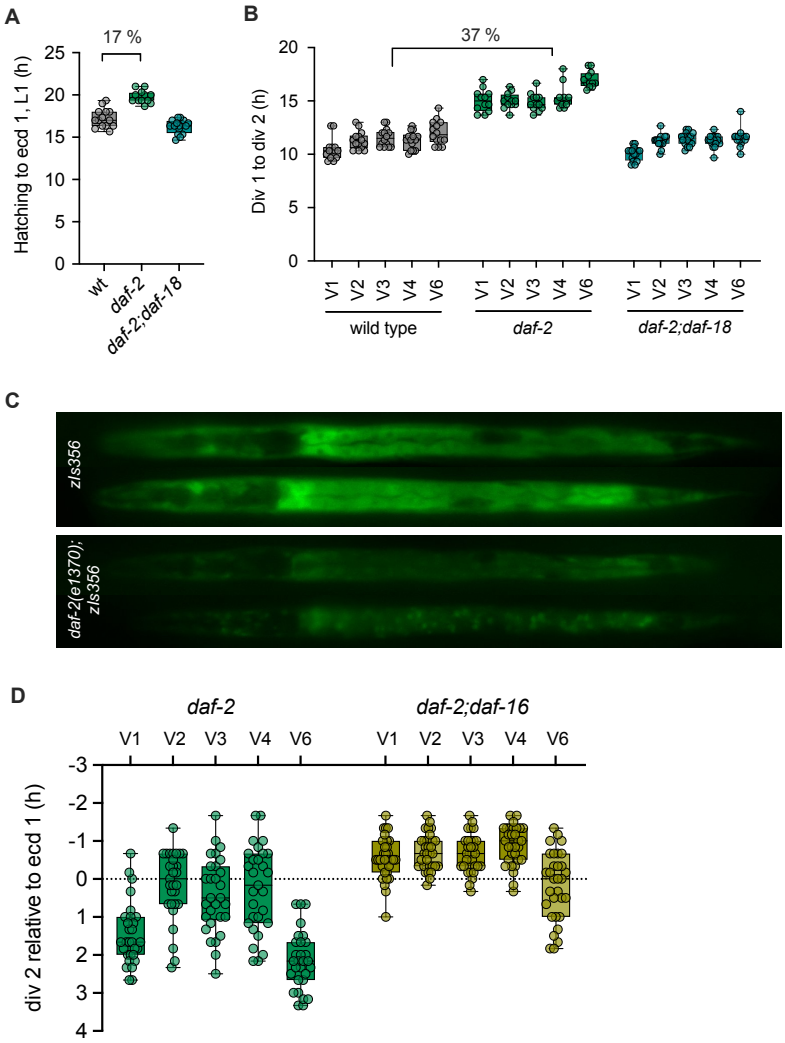

Figure S4. (Related to figure 5). (A) Duration of L1 measured by microscopic monitoring of hatching and ecdysis for the wild-type strain, the *daf-2 mutant* and *daf-2;daf-18*. **(B)** Duration of the interval from the first to second seam cell division in the same strains. The percentages at the top indicate the delay of the *daf-2* mutant relative to the wild-type. **(C)** Representative images of DAF-16::GFP on the wild type and *daf-2(e1370)* backgrounds. **(D)** Timing of seam cell division (div 2) relative to ecd 1 for the *daf-2* mutant and the double mutant *daf-2;daf-16*. Colored circles show values for individual larvae.

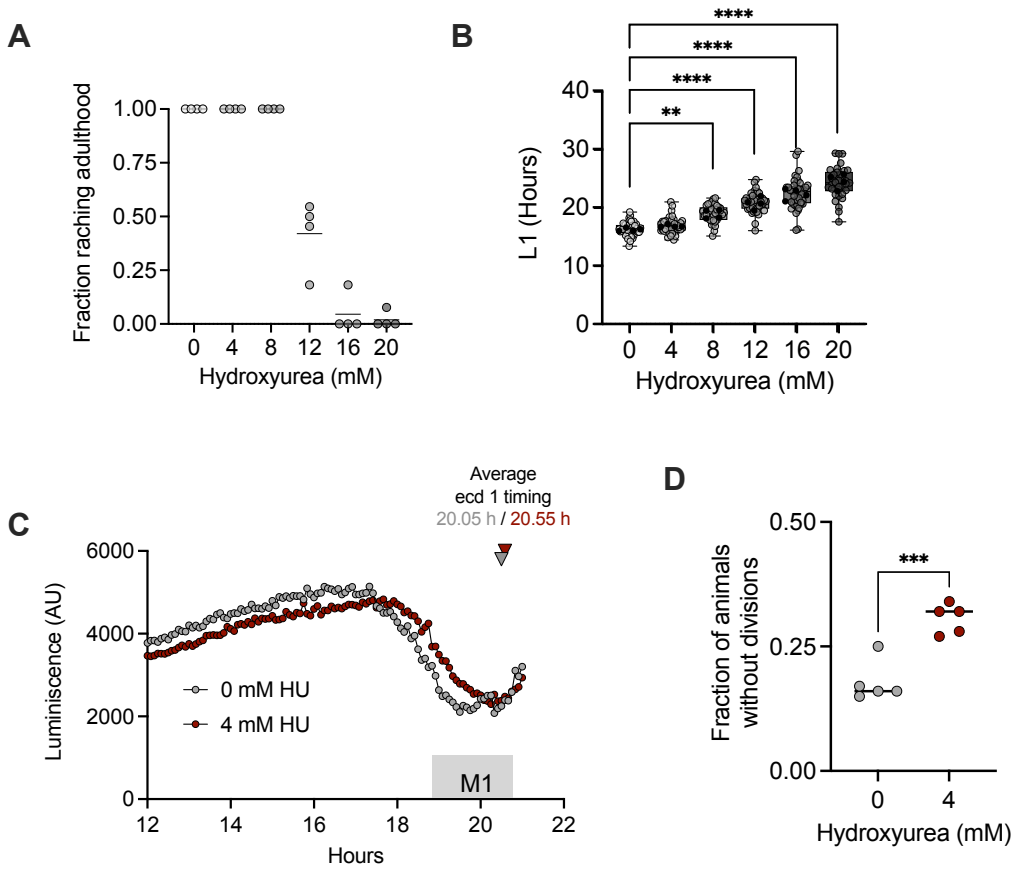

Figure S5. (Related to figure 6). (A) Fraction of animals that reach adults after treatment with different concentration of HU from L1, in four independent experiments. **(B)** Duration of the stage L1 after treatment with different concentrations of HU in four independent experiments. We performed One-way ANOVA followed by Dunnet´s multiple comparisons to test differences between each of the treatments and the untreated larvae. Complete statistics results are shown in Supplementary Table S3. Differences are marked as ** $p<0.005$, **** $p<0.0001$. Grey circles show values for individual larvae and black dots show the average of each experiment. **(C)** Representative traces of luminescence of populations of larvae treated with HU and control larvae. The average ecdysis timing is precisely calculated from individual larvae. **(D)** Fraction of animals without seam cell divisions for larvae treated with 4 mM HU and control larvae. Complete statistical analysis is shown in File S1.

Table S1. List of bacterial and *C. elegans* strains

Strains	Source	Identifier
Bacteria		
E. coli OP50-1	*Caenorhabditis* Genetics Center	OP50-1
E. coli HT115(DE3) pL4440	Rual et al., 2004	
E. coli HT115(DE3) *mpk-1* RNAi	Ahringer library	
Caenorhabditis elegans		
sevIs1[Psur-5::luc+::gfp]X	Olmedo et al., 2020	MRS387
daf-2(e1370)III; sevIs1 [Psur-5::luc+::gfp]X	Olmedo et al., 2020	MRS434
daf-2(e1368)III; sevIs1 [Psur-5::luc+::gfp]X	This study	MOL162
daf-2(m41)III; sevIs1[Psur-5::luc+::gfp]X	This study	MOL129
daf-2(m577)III; sevIs1 [Psur-5::luc+::gfp]X	This study	MOL164
daf-2(m596)III; sevIs1 [Psur-5::luc+::gfp]X	This study	MOL166
daf-2(e1391)III; sevIs1[Psur-5::luc+::gfp]X	This study	MOL353
daf-2(e979)III; sevIs1[Psur-5::luc+::gfp]X	This study	MOL453
daf-2(hq363[daf-2::degron::mNeonGreen]) III, sevIs1[Psur-5::luc+::gfp]X	This study	MOL480
daf-2(hq363[daf-2::degron::mNeonGreen]) III, ieSi57 [eft-3p::TIR1::mRuby::unc-54 3' UTR + Cbr-unc-119(+)] II; sevIs1[Psur-5::luc+::gfp]X	This study	MOL481
daf-16(mu86)I; sevIs1 [Psur-5::luc+::gfp]X	Olmedo et al., 2020	MRS424
daf-2(e1370)III; daf-16(mu86)I; sevIs1[Psur-5::luc+::gfp]X	Olmedo et al., 2020	MOL56
daf-2(e1391)III; daf-16(mu86)I; sevIs1[Psur-5::luc+::gfp]X	This study	MOL346
daf-2(e979)III; daf-16(mu86); sevIs1[Psur-5::luc+::gfp]X	This study	MOL454
age-1 (mg305)II; sevIs1[Psur-5::luc+::gfp]X	This study	MOL370
age-1(mg305)II; daf-16(mu86); sevIs1[Psur-5::luc+::gfp]	This study	MOL417
daf-18(ok480) IV x sevIs1[Psur-5::luc+::gfp]X	This study	MOL267
daf-2(e1370); daf-18(ok480) IV x sevIs1[Psur-5::luc+::gfp]X	This study	MOL315
daf-16(mu86)I; daf-18(ok480)IV; sevIs1[Psur-5::luc+::gfp]X	This study	MOL433
daf-2(e1370)III; daf-16(mu86)I; daf-18(ok480)IV; sevIs1[Psur-5::luc+::gfp]X	This study	MOL434
daf-18(e1375)IV; sevIs1[Psur-5::luc+::gfp]X	This study	MOL376
daf-2(e1370)III; daf-18(e1375)IV; sevIs1[Psur-5::luc+::gfp]X	This study	MOL377
let-60(ga89)IV;sevIs1[Psur-5::luc+::gfp]X	This study	MOL231
let-60(ga89)IV; daf-2(e1370)III; sevIs1[Psur-5::luc+::gfp]X	This study	MOL331
daf-18(ok480)IV; let-60(ga89)IV;sevIs1[Psur-5::luc+::gfp]X	This study	MOL603
let-60(ga89)IV; daf-18(ok480)IV; daf-2(e1370)III; sevIs1[Psur-5::luc+::gfp]X	This study	MOL569
matIs38 [Pscm::CYB-1 DB-mCherry::unc-54 3' UTR; Pscm::NLS-GFP::tbb-2 3' UTR; Pmyo-2::GFP]	Dr. Matilde Galli Hubrecht Institute	GAL69
daf-2(e1370)III; matIs38 [Pscm::CYB-1 DB-mCherry::unc-54 3' UTR; Pscm::NLS-GFP::tbb-2 3' UTR; Pmyo-2::GFP]	This study	MOL185
daf-2(e1370); daf-18(ok480)IV; matIs38 [Pscm::CYB-1 DB-mCherry::unc-54 3' UTR; Pscm::NLS-GFP::tbb-2 3' UTR; Pmyo-2::GFP]	This study	MOL367
daf-2(e1370)III; sevIs1[Psur-5::luc+::gfp]X; matIs38 [Pscm::CYB-1 DB-mCherry::unc-54 3' UTR; Pscm::NLS-GFP::tbb-2 3' UTR; Pmyo-2::GFP]	This study	MOL344
daf-2(e1370)III; daf-16(mu86)I; sevIs1[Psur-5::luc+::gfp]X; matIs38 [Pscm::CYB-1 DB-mCherry::unc-54 3' UTR; Pscm::NLS-GFP::tbb-2 3' UTR; Pmyo-2::GFP]	This study	MOL435
zIs356[Pdaf-16::daf-16a/b-gfp; rol-6] IV	CGC	TJ356
daf-2(e1370)III; zIs356[Pdaf-16::daf-16a/b::gfp; rol-6]	Olmedo et al., 2020	MOL72

Table S2. Strains used, number of larvae, and experimental replicates.

Main figures				
	Label	**Strain**	**n larvae (at least)**	**N replicates**
1E	wt	MRS387	33	3
	daf-2	MRS434	30	3
1F,G		MRS434	56	5
2A,B	wt	MRS387	55	5
	e1370	MRS434	56	5
	e1368	MOL162	56	5
	m41	MOL129	53	5
	m577	MOL164	60	5
	m596	MOL166	56	5
2C,D	wt	MRS387	63	4
	e1370	MRS434	62	4
	e1391	MOL353	43	4
	e979	MOL453	28	4
2E,F	wt	MRS387	21	3
	daf-2(e1370)	MRS434	22	3
	DAF-2::AID;TIR1 / 2 mM NAA	MOL481	81	3
	DAF-2::AID;TIR1 / 4 mM NAA	MOL481	74	3
3B,C	wt	MRS387	95	8
	daf-16	MRS424	101	8
	daf-2	MRS434	77	8
	daf-2;daf-16	MOL56	111	8
3D,E	wt	MRS387	64	7
	daf-16	MRS424	54	7
	daf-2	MRS434	92	7
	daf-2;daf-16	MOL56	81	7
	age-1	MOL370	55	7
	age-1daf-16	MOL417	78	7
3F,G	wt	MRS387	62	4
	daf-16	MRS424	49	4
	daf-18	MOL267	54	4
	daf-16;daf-18	MOL433	45	4
	daf-2	MRS434	50	4
	daf-2;daf-16	MOL56	42	4
	daf-2;daf-18	MOL315	60	4
	daf-2;daf-16;daf-18	MOL434	62	4
4A,B,F	*control*	MOL6/pL4440	98	5
	mpk-1 RNAi	MOL6/*mpk-1* RNAi	101	5
4C-E	wt	MRS387	76	5
	let-60(gf)	MOL231	62	5
	daf-2	MRS434	72	5
	daf-2;let-60	MOL331	42	5
	daf-18	MOL267	63	5
	daf-18;let-60	MOL603	11	5
	daf-2;daf-18	MOL315	71	5
	daf-2;daf-18;let-60	MOL569	81	5

5B,C	*wt*	MOL159	15	4
	daf-2	MOL185	12	4
	daf-2;daf-18	MOL367	16	4
6A	L2a	MOL344	9	4
	I2	MOL344	10	4
	I2 after L2a	MOL344	9	4
6B-C	wt AL	MRS387	20	3
	wt CR	MRS387	18	3
	daf-2 AL	MRS434	23	3
	daf-2 CR	MRS434	20	3
6D-E	0 mM HU	MRS387	44	4
	4 mM HU	MRS387	43	4
6F-G	12 ºC	MRS387	38	3
	16 ºC	MRS387	61	3
	20 ºC	MRS387	40	3
	22 ºC	MRS387	38	3